Am J Physiol Endocrinol Metab 286: E280–E285, 2004.
First published October 7, 2003; 10.1152/ajpendo.00380.2003.

Overexpression of constitutively activated glutamate dehydrogenase induces insulin secretion through enhanced glutamate oxidation

Takatoshi Anno,[1] Shunsuke Uehara,[2] Hideki Katagiri,[3] Yasuharu Ohta,[1] Kohei Ueda,[1] Hiroyuki Mizuguchi,[4] Yoshinori Moriyama,[2] Yoshitomo Oka,[3] and Yukio Tanizawa[1]

[1]Division of Molecular Analysis of Human Disorders, Department of Bio-Signal Analysis, Yamaguchi University Graduate School of Medicine, Ube, Yamaguchi 755-8505; [2]Department of Biochemistry, Faculty of Pharmaceutical Sciences, Okayama University, Okayama 700-8530; [3]Division of Molecular Metabolism and Diabetes, Department of Internal Medicine, Tohoku University Graduate School of Medicine, Sendai 980-8574; and [4]Division of Cellular and Gene Therapy Products, National Institute of Health Sciences, Tokyo 158-8501, Japan

Submitted 25 August 2003; accepted in final form 2 October 2003

Anno, Takatoshi, Shunsuke Uehara, Hideki Katagiri, Yasuharu Ohta, Kohei Ueda, Hiroyuki Mizuguchi, Yoshinori Moriyama, Yoshitomo Oka, and Yukio Tanizawa. Overexpression of constitutively activated glutamate dehydrogenase induces insulin secretion through enhanced glutamate oxidation. *Am J Physiol Endocrinol Metab* 286: E280–E285, 2004. First published October 7, 2003; 10.1152/ajpendo.00380.2003.—Glutamate dehydrogenase (GDH) catalyzes reversible oxidative deamination of L-glutamate to α-ketoglutarate. Enzyme activity is regulated by several allosteric effectors. Recognition of a new form of hyperinsulinemic hypoglycemia, hyperinsulinism/hyperammonemia (HI/HA) syndrome, which is caused by gain-of-function mutations in GDH, highlighted the importance of GDH in glucose homeostasis. GDH266C is a constitutively activated mutant enzyme we identified in a patient with HI/HA syndrome. By overexpressing GDH266C in MIN6 mouse insulinoma cells, we previously demonstrated unregulated elevation of GDH activity to render the cells responsive to glutamine in insulin secretion. Interestingly, at low glucose concentrations, basal insulin secretion was exaggerated in such cells. Herein, to clarify the role of GDH in the regulation of insulin secretion, we studied cellular glutamate metabolism using MIN6 cells overexpressing GDH266C (MIN6-GDH266C). Glutamine-stimulated insulin secretion was associated with increased glutamine oxidation and decreased intracellular glutamate content. Similarly, at 5 mmol/l glucose without glutamine, glutamine oxidation also increased, and glutamate content decreased with exaggerated insulin secretion. Glucose oxidation was not altered. Insulin secretion profiles from GDH266C-overexpressing isolated rat pancreatic islets were similar to those from MIN6-GDH266C, suggesting observation in MIN6 cells to be relevant in native β-cells. These results demonstrate that, upon activation, GDH oxidizes glutamate to α-ketoglutarate, thereby stimulating insulin secretion by providing the TCA cycle with a substrate. No evidence was obtained supporting the hypothesis that activated GDH produced glutamate, a recently proposed second messenger of insulin secretion, by the reverse reaction, to stimulate insulin secretion.

hypoglycemia; hyperinsulinism/hyperammonemia syndrome; islet of Langerhans

THE MITOCHONDRIAL MATRIX ENZYME glutamate dehydrogenase (GDH; EC 1.4.1.3) catalyzes reversible oxidative deamination of L-glutamate to α-ketoglutarate with NAD(P) as a cofactor. The activity of this enzyme is regulated positively and negatively by several allosteric effectors, including amino acids (leucine, isoleucine, valine, methionine), ADP, and GTP. In pancreatic β-cells, GDH has been suggested to be involved in the regulation of insulin secretion, especially leucine-stimulated insulin secretion (18, 19). The importance of GDH in glucose homeostasis is also evident from recent findings that gain-of-function mutations in the GLUD1 gene, which encodes GDH, cause hyperinsulinism /hyperammonemia (HI/HA) syndrome (9, 20, 21, 22, 25, 29).

Previously, we identified a GLUD1 gene mutation, Y266C, in a patient with HI/HA syndrome (22). The activity of the mutant GDH (GDH266C) was constitutively elevated, and allosteric regulations by ADP and GTP were severely impaired. Using GDH266C as a tool, we showed unregulated elevation of GDH activity in MIN6 insulinoma cells to render the cells responsive to glutamine. Glutamine stimulated insulin secretion from these cells in the absence of leucine, an allosteric activator of GDH. We also demonstrated insulin secretion to be exaggerated in these cells at low glucose concentrations (22). Glutamine alone, to which the plasma membrane is permeable and which is readily converted to glutamate intracellularly, does not normally stimulate insulin release. However, it remarkably stimulates insulin secretion in the presence of leucine. It is generally accepted that, in pancreatic β-cells, activation of GDH by allosteric effectors, such as leucine, enhances glutamate oxidation and increases ATP production by providing the tricarboxylic acid (TCA) cycle with α-ketoglutarate and thereby stimulates insulin secretion (18, 19). Physiologically, GDH is also suggested to play an important role in basal insulin secretion (2, 5). Our previous observations (22) in MIN6 cells are in good agreement with this theory.

On the other hand, mitochondrially derived glutamate was suggested to be a second messenger in glucose-stimulated insulin secretion, acting directly on insulin-secretory granules (4, 11, 17). This theory assumes reverse flux through GDH in the direction of glutamate formation, and glutamate-induced insulin secretion was suggested to correlate with the level of GDH expression (4, 10). However, this hypothesis is controversial and has been contradicted by other studies (2, 8). Furthermore, it was recently demonstrated that cellular glutamate content did not correlate with the amplification of insulin secretion (1, 7). Most previous studies have investigated the role of GDH in insulin secretion by activating intracellular

Address for reprint requests and other correspondence: Y. Tanizawa, Div. of Molecular Analysis of Human Disorders, Dept. of Bio-Signal Analysis, Yamaguchi Univ. Graduate School of Medicine, Minami-Kogushi Ube, Yamaguchi 755-8505, Japan (E-mail: tanizawa@yamaguchi-u.ac.jp).

The costs of publication of this article were defrayed in part by the payment of page charges. The article must therefore be hereby marked "*advertisement*" in accordance with 18 U.S.C. Section 1734 solely to indicate this fact.

0193-1849/04 $5.00 Copyright © 2004 the American Physiological Society

American Journal of Physiology - Endocrinology and Metabolism

GDH with allosteric activators such as leucine or β-2-aminobicyclo[2.2.1]heptane-2-carboxylic acid. Identification of constitutively activated mutant GDH (GHD266C) enabled us to study the effects of elevated intracellular GDH activity on insulin secretion more directly by introducing the mutant enzyme into cells. Our present study was designed to investigate directly the correlations among insulin secretion, GDH activity, and cellular glutamate metabolism. We also studied changes in insulin secretion profiles caused by unregulated elevation of GDH activity in native β-cells to confirm the physiological relevance of our findings in MIN6 cells. Our results further clarify the role of GDH in the regulation of insulin secretion and provide insights into the pathophysiology of the HI/HA syndrome.

MATERIALS AND METHODS

Analysis of glutamine and glucose oxidation. MIN6 cells overexpressing the mutant GDH via retrovirus-mediated gene transfer (MIN6-GDH266C) and control lacZ-overexpressing cells (MIN6-lacZ) were used for these experiments (22). Cells were seeded onto a 6-cm dish at a concentration of 4.0×10^6 cells/dish and cultured in DMEM-MIN6 medium (Sigma, St. Louis, MO) containing 25 mmol/l glucose supplemented with 15% heat-inactivated fetal calf serum, 72 μmol/l β-mercaptoethanol, 50 U/ml penicillin G, and 50 μg/ml streptomycin. Sixty hours later, glutamine or glucose oxidation was assayed. After a 30-min preincubation in HEPES-balanced Krebs-Ringer bicarbonate buffer (HB-KRBB; in mmol/l: 10 HEPES, 120 NaCl, 4.7 KCl, 1.2 $MgSO_4$, 1.2 KH_2PO_4, 20 $NaHCO_3$, and 2 $CaCl_2$, pH 7.4) containing 0.5% BSA and 5 mmol/l glucose, radioactive L-[U-^{14}C]glutamine (0.05 μCi, 261 Ci/mol; Amersham, Buckinghamshire, UK) or radioactive D-[6-^{14}C]glucose [0.04 μCi (for 5 mmol/l glucose) or 0.20 μCi (for 25 mmol/l glucose), 58.0 Ci/mol; Amersham] was added to 4 ml of fresh HB-KRBB containing 0.5% BSA and various concentrations of glutamine or glucose. Then, MIN6-GDH266C or MIN6-lacZ cells in the culture dishes were placed immediately in sealed glass containers (7 cm diameter × 10 cm height) filled with 100% oxygen and incubated for 30 min (glutamine oxidation) or 1 h (glucose oxidation) at 37°C. At completion of the incubations, 0.5 ml of 10% $HClO_4$ was added to the medium by means of a long 21-gauge needle through rubber stoppers on the top of the container, allowing CO_2 gas (containing radioactive [^{14}C]CO_2) to evaporate and be trapped in 2 ml of 10% KOH solution in a small glass cup suspended above the medium in a sealed glass container. The glass containers were incubated for another 30 min, and the KOH solution was then transferred to scintillation vials containing 10 ml of Aquasol-2 (PerkinElmer, Boston, MA), and radioactivity was measured with a liquid scintillation counter. With this system, 90.7 ± 1.2% (mean ± SE; $n = 3$) of CO_2 gas, evaporating from the medium containing 0.5 μCi NaH[^{14}C]O_3 (Amersham), was trapped in KOH solution.

Measurement of intracellular glutamate content. MIN6-GDH266C and control MIN6-lacZ cells were seeded onto six-well plates at a concentration of 1.8×10^6 cells/well and cultured in DMEM-MIN6 medium. Sixty hours later, glutamate contents were assayed. After a 30-min preincubation in HB-KRBB containing 0.5% BSA and 5 mmol/l glucose, the preincubation buffer was replaced with fresh HB-KRBB containing 0.5% BSA and various concentrations of glutamine or glucose, and the cells were incubated for an additional hour at 37°C. At the end of the incubation, the cells were quickly washed on ice with ice-cold HB-KRBB, and 1 ml of 6% perchloric acid was immediately added. The cells were then collected and sonicated on ice. After centrifugation at 15,000 rpm for 5 min, the supernatant (800 μl) was collected, and 275 μl of 30% KOH were added. White precipitates were removed by brief centrifugation, and the supernatant was kept at −80°C for the glutamate measurement. Cells in one of the wells were homogenized in PBS and used for protein determination. The amount of glutamate was determined, using an aliquot of the cell extract, by high-performance liquid chromatography with precolumn *o*-phthalaldehyde derivatization, separation on a reverse-phase Resolve C18 column (3.9 × 150 mm; Waters, Toronto, ON, Canada), and fluorescence detection (3, 27, 28).

Construction of recombinant adenoviruses and adenovirus-mediated gene transfer. pcDNA3-hGDH-WT and pcDNA3-hGDH266C (22) were digested with *Not*I and *Sna*BI. The fragments containing GDH cDNA were then ligated into *Not*I- and *Sna*BI-digested pShuttle vectors (14, 15). The resultant plasmids, pShuttle-hGDH-WT and pShuttle-hGDH266C, were then digested with I-*Ceu*I/PI-*Sce*I and ligated into I-*Ceu*I/PI-*Sce*I-digested pAdHM4 (14, 15) to produce pAd-hGDH-WT and pAd-hGDH266C. They were then linearized with *Pac*I and transfected into 293 human embryonic kidney cells with FuGENE6 (Roche Diagnostics, Mannheim, Germany) according to the manufacturer's instructions. Recombinant adenoviruses expressing GDH-WT and GDH266C (Ad-hGDH-WT and Ad-hGDH266C) were thus obtained and amplified via infection of 293 cells. As a control, we also constructed an adenoviral vector to express enhanced green fluorescent protein (eGFP; Ad-eGFP). Titers of the recombinant adenovirus stocks were 6.0×10^7 (Ad-hGDH-WT), 5.5×10^7 (Ad-hGDH266C), and 9.5×10^7 plaque-forming units (pfu)/ml (Ad-eGFP).

Pancreatic islets were isolated by collagenase digestion as described previously (6, 24). Isolated islets were cultured on a 60-mm tissue culture dish with RPMI 1640 medium containing 11 mmol/l glucose supplemented with 10% fetal calf serum, 50 U/ml penicillin, and 50 μg/ml streptomycin (RPMI-islet) and maintained at 37°C in humidified 5% CO_2-95% air. Twenty-four to thirty-six hours after isolation, groups of 50–100 islets were incubated with the recombinant adenoviruses at a multiplicity of infection (moi) of $\sim 4 \times 10^5$ pfu/islet. After a 1-h incubation with the adenovirus at 37°C, the medium was removed, and the islets were washed once with phosphate-buffered saline (PBS). The islets were then further incubated on a 60-mm tissue culture dish with RPMI-islet medium. Experiments were performed 24 h after infection.

GDH enzyme assay. COS-7 cells and isolated pancreatic islets were infected with recombinant adenoviruses at an moi of ~10 pfu/cell or 4×10^5 pfu/islet, respectively. Forty-eight (COS-7) or 24 (islets) h after the infection, cells were washed, suspended in PBS, and sonicated to prepare crude cell extract. GDH activity was measured by the oxidation of NADH ($\epsilon_{340\ nm} = 6.22 \times 10^3$ mol·l^{-1}·cm^{-1}), as described previously (26), with a Beckman Coulter (Fullerton, CA) Spectrophotometer model DU-640 at 25°C. The assay solution (1 ml) consisted of 10 mmol/l Tris-acetate (pH 8.0), 10 μmol/l EDTA, 100 μmol/l NADH, 50 mmol/l NH_4Cl, and 5 mmol/l α-ketoglutarate. ADP, GTP, or leucine was added to the solution at various concentrations. The reaction was started by adding appropriate amounts (30–50 μl) of cell extracts, and the decrease in absorbance at 340 nm was measured for 5 min. During this incubation period, the reaction was linear, and there was no indication of GTP hydrolysis, substrate depletion, or product saturation. The activity was determined in duplicate for each sample.

Analysis of insulin secretion. Groups of 10–30 islets overexpressing the mutant GDH (Islets-GDH266C) and eGFP (Islets-eGFP) via adenovirus-mediated gene transfer were used for each assay. Insulin secretion was examined by the static incubation method (23, 24). In brief, after a 30-min preincubation in HB-KRBB supplemented with 0.5% BSA and 5 mmol/l glucose, the preincubation buffer was replaced with fresh HB-KRBB containing 0.5% BSA and various concentrations of glutamine or glucose. After an additional 30-min incubation at 37°C, the buffer was collected, and immunoreactive insulin was measured by radioimmunoassay using rat insulin (Linco Research, St. Charles, MO) as a standard. The amounts of secreted insulin were corrected by the amounts of cell protein in each well.

American Journal of Physiology – Endocrinology and Metabolism

RESULTS

Glutamine and glucose metabolism in MIN6-GDH266C cells. We investigated the metabolic changes associated with elevated GDH activity. We used MIN6-GDH266C as a model. When the cells were incubated in the presence of glutamine (1 mmol/l) with a tracer of L-[U-^{14}C]glutamine, glutamine oxidation was increased in MIN6-GDH266C compared with control MIN6-lacZ ($P < 0.02$, unpaired *t*-test; Fig. 1*A*). In agreement with the enhanced glutamine oxidation, intracellular glutamate content in MIN6-GDH266C was lower than that in MIN6-lacZ ($P < 0.01$ at 1.0 mmol/l; Fig. 1*B*).

At low glucose concentrations (without exogenous glutamine), insulin secretion was augmented in MIN6-GDH266C (22). We then studied metabolic changes under these conditions. Glucose oxidation did not differ between MIN6-GDH266C and MIN6-lacZ [4.0 ± 0.7 vs. 4.0 ± 0.9 pmol/μg protein at 5 mmol/l glucose ($P > 0.9$; Fig. 2*A*) and 7.9 ± 2.0 vs. 6.8 ± 1.9 pmol/μg protein at 25 mmol/l glucose ($P > 0.6$; unpaired *t*-test)]. Cellular glutamine oxidation, however, was significantly enhanced in MIN6-GDH266C [46.7 ± 1.2 vs. 27.2 ± 1.6 pmol/μg protein at 5 mmol/l glucose ($P < 0.001$; Fig. 2*B*) and 31.7 ± 4.1 vs. 16.4 ± 2.0 pmol/μg protein at 25 mmol/l glucose ($P < 0.03$; unpaired *t*-test)]. The corresponding intracellular glutamate content was decreased in MIN6-GDH266C compared with that in MIN6-lacZ [10.3 ± 2.0 vs. 25.4 ± 2.3 pmol/μg protein at 5 mmol/l glucose ($P < 0.002$; Fig. 2*C*) and 14.2 ± 1.3 vs. 36.6 ± 2.1 pmol/μg protein at 25 mmol/l glucose ($P < 0.001$; unpaired *t*-test)]. These results indicate that elevated GDH activity enhances glutamine oxidation and probably increases ATP synthesis via the TCA cycle, thereby stimulating insulin secretion.

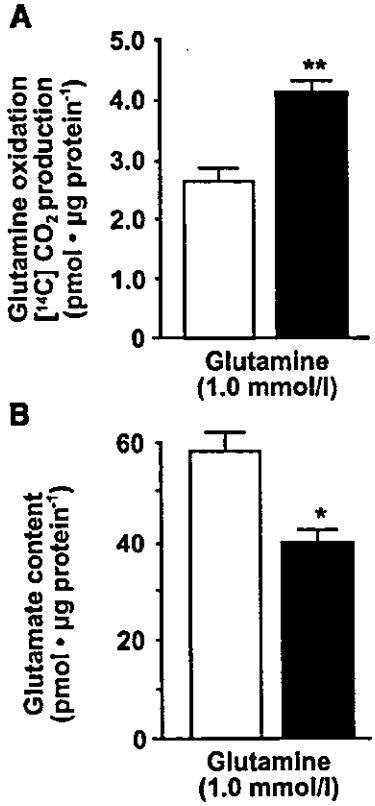

Fig. 1. Glutamine oxidation and glutamate content in MIN6 cells incubated in the presence of glutamine. *A*: glutamine oxidation. MIN6 cells overexpressing consitutively activated mutant glutamate dehydrogenase (GDH; MIN6-GDH266C; filled bar) and MIN6 cells overexpressing lacZ (MIN6-lacZ; open bar) were preincubated in HEPES-balanced Krebs-Ringer bicarbonate buffer (HB-KRBB) with 5 mmol/l glucose for 30 min at 37°C, followed by incubation in HB-KRBB with 1 mmol/l L-[U-^{14}C]glutamine for 30 min at 37°C. [^{14}C]CO_2 produced by the MIN6 cells was trapped in KOH solution and radioactivity determined by liquid scintillation counting. Data are means ± SE of 3 experiments. $^{**}P < 0.02$ for comparison between MIN6-GDH266C and MIN6-lacZ (unpaired Student's *t*-test). *B*: glutamate contents. MIN6-GDH266C (filled bar) and MIN6-lacZ (open bar) cells were preincubated at 37°C in HB-KRBB with 5 mmol/l glucose for 30 min, followed by incubation at 37°C in the presence of 1 mmol/l glutamine for 1 h. Immediately after incubation, cells were quickly homogenized in ice-cold perchloric acid solution. The solution was neutralized and the supernatant saved at −80°C for the glutamate assay. Glutamate content was determined by HPLC. Data are means ± SE of 5 experiments. $^{*}P < 0.01$ for comparison between MIN6-GDH266C and MIN6-lacZ (unpaired Student's *t*-test).

Characterizations of GDH266C expressed in COS-7 cells and in isolated rat pancreatic islets. To overexpress GDH266C in isolated rat pancreatic islets, we constructed a recombinant adenovirus, Ad-hGDH266C. As we previously demonstrated using the enzyme expressed in COS-7 cells (22), basal activity (activity in the absence of allosteric effecters) of GDH266C was elevated, and inhibition by GTP and activation by ADP were blunted compared with those of the wild-type enzyme. Here, we further characterized activation by leucine by using COS-7 cell extracts in which wild-type GDH or GHD266C was overexpressed by adenovirus-mediated gene transduction. Activation of GDH266C by leucine was only twofold (from 2,850 ± 120 to 5,520 ± 190 nmol NADH·mg protein^{-1}·min^{-1} at 3 mmol/l leucine), whereas that of wild-type GDH was more than 35-fold (from 130 ± 20 to 4,670 ± 70 nmol NADH·mg protein^{-1}·min^{-1} at 3 mmol/l leucine). Maximal activity of GDH266C in the presence of leucine was nearly the same as that of the wild-type enzyme in the crude cell extracts, although analysis of the purified enzyme was necessary for the strict quantitative comparison.

Next, we overexpressed GDH266C in isolated islets (Islets-GDH266C) using the adenovirus-mediated gene transfer system to investigate the role of GDH in native β-cells. Islets overexpressing eGFP (Islets-eGFP) were used as a control. Transfer of exogeneous genes with adenovirus vector to islets was very efficient, and most of the islet cells expressed eGFP when they were infected with Ad-eGFP, as confirmed by observation under fluorescence microscopy (Ref. 24 and data not shown). The basal GDH activities in the crude extracts of Islets-eGFP and Islets-GDH266C were 20 ± 3 and 2,890 ± 670 nmol NADH·mg protein^{-1}·min^{-1}, respectively, when activity was measured without allosteric effectors in the reaction mixture (Table 1). As expected, ADP activated GDH activity 20-fold in the crude extract of Islets-eGFP (510 ± 50 nmol NADH·mg protein^{-1}·min^{-1} at 200 μmol/l ADP), whereas activation in the extract of Islets-GDH266C was less than twofold (4,570 ± 650 nmol NADH·mg protein^{-1}·min^{-1} at 200 μmol/l ADP). GTP did not inhibit GDH activity in Islets-GDH266C (2,840 ± 600 nmol NADH·mg protein^{-1}·min^{-1} at 25 μmol/l GTP). Therefore, in Islets-GDH266C, GDH activity was constitutively elevated.

Profiles of insulin secretion from Islets-GDH266C. It is known that in normal pancreatic β-cells glutamine stimulates

American Journal of Physiology – Endocrinology and Metabolism

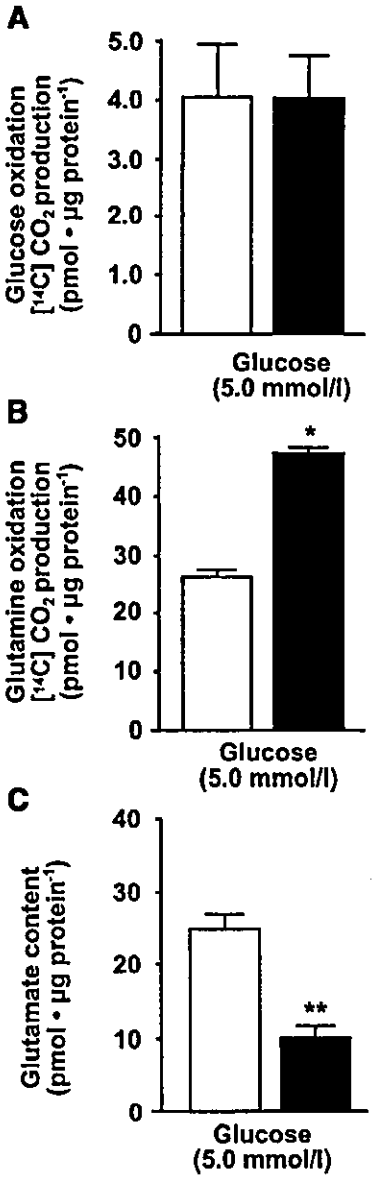

Fig. 2. Glutamine oxidation and glutamate content in MIN6 cells incubated in the presence of 5 mmol/l glucose. *A*: glucose oxidation. MIN6-GDH266C (filled bar) and MIN6-lacZ (open bar) cells were preincubated in HB-KRBB with 5 mmol/l glucose for 30 min at 37°C, followed by incubation in HB-KRBB with 5 mmol/l D-[6-^{14}C]glucose for 1 h at 37°C. [^{14}C]CO_2 produced by the MIN6 cells was trapped in KOH solution and radioactivity determined by liquid scintillation counting. Data are means ± SE of 6 experiments. *B*: glutamine oxidation. MIN6-GDH266C (filled bar) and MIN6-lacZ (open bar) cells were preincubated at 37°C in HB-KRBB with 5 mmol/l glucose for 30 min, followed by incubation at 37°C for 30 min in the presence of 5 mmol/l glucose and a tracer of radioactive L-[U-^{14}C]glutamine. Radioactive [^{14}C]CO_2 produced by the MIN6 cells was trapped in KOH solution and radioactivity determined by liquid scintillation counting. Data are means ± SE of 3 experiments. *$P < 0.001$ for comparison between MIN6-GDH266C and MIN6-lacZ (unpaired Student's *t*-test). *C*: glutamate contents. MIN6-GDH266C (filled bar) and MIN6-lacZ (open bar) cells were preincubated at 37°C in HB-KRBB with 5 mmol/l glucose for 30 min, followed by incubation at 37°C in the presence of 5 mmol/l glucose for 1 h. After incubation, glutamate contents were measured as described in Fig. 1. Data are means ± SE of 5 experiments. **$P < 0.002$ for comparison between MIN6-GDH266C and MIN6-lacZ (unpaired Student's *t*-test).

Table 1. *GDH activity in Islets-GDH266C and Islets-eGFP*

ADP, µmol/l	GTP, µmol/l	GDH Activity, nmol NADH·mg protein^{-1}·min^{-1} Islets-eGFP	Islets-266C
0	0	20±3	2,890±670
200	0	510±50	4,570±650
0	25	*	2,840±600

Values are means ± SE; $n = 3$. GDH, glutamate dehydrogenase; Islets-GDH266C, islets overexpressing a constitutively activated mutant GDH; Islets-eGFP, islets overexpressing enhanced green fluorescent protein (control). *Below assay sensitivity.

insulin secretion only in the presence of leucine, an allosteric activator of GDH. As shown in Fig. 3*A*, glutamine alone did not stimulate insulin secretion from Islets-eGFP, as was observed with intact islets. On the other hand, it stimulated insulin secretion from Islets-GDH266C in a dose-dependent manner.

Glucose-stimulated insulin secretion was also studied. Insulin secretion from Islets-GDH266C was significantly exaggerated at low glucose concentrations compared with control Islets-eGFP [0.16 ± 0.03 (Islets-eGFP) vs. 0.34 ± 0.09 ng insulin/µg protein (Islets-GDH266C) at 2 mmol/l glucose ($P < 0.05$, $n = 16$); 0.29 ± 0.06 (Islets-eGFP) vs. 0.48 ± 0.07 ng insulin/µg protein (Islets-GDH266C) at 5 mmol/l glucose ($P < 0.001$, $n = 15$); 0.55 ± 0.08 (Islets-eGFP) vs. 0.78 ± 0.15 ng insulin/µg protein (Islets-GDH266C) at 8 mmol/l glucose ($P < 0.05$, $n = 14$); paired *t*-test] but not at higher glucose concentrations (Fig. 3*B*).

DISCUSSION

A mutant GDH, GHD266C, which was identified in a Japanese patient with HI/HA syndrome, is a constitutively activated enzyme: basal activity is elevated, and activation by ADP and inhibition by GTP are blunted compared with the wild-type enzyme (22). In addition, we have herein demonstrated activation by leucine also to be blunted. It has been suggested that ADP binds to and activates GDH by opening the catalytic cleft of the enzyme (16). Leucine is thought to bind at the active site (26). It is possible that in GDH266C the catalytic cleft is almost fully open in the basal state, such that binding of ADP or leucine only minimally activates this mutant enzyme. We used the GDH266C, rather than wild-type GDH, as a tool to examine the effects of elevated cellular GDH activity in the regulation of insulin secretion, because with this mutant, GDH activity is thought to be elevated regardless of phosphate potential (GTP and ATP-to-ADP and P_i ratio) (2, 5) in the cells.

We previously demonstrated glutamine to stimulate insulin secretion from MIN6 cells overexpressing GDH266C (MIN6-GDH266C) in the absence of leucine. In addition, and very interestingly, insulin secretion from MIN6-GDH266C cells was exaggerated at low glucose concentrations (2–5 mmol/l) in the absence of glutamine in the incubation buffer (22). To investigate the mechanism by which elevated cellular GDH activity leads to the stimulation of insulin secretion, we studied changes in glutamate metabolism in cells in which GDH activity was constitutively elevated.

In association with the stimulation of insulin secretion by glutamine, cellular glutamine oxidation was elevated (Fig. 1*A*),

American Journal of Physiology = Endocrinology and Metabolism

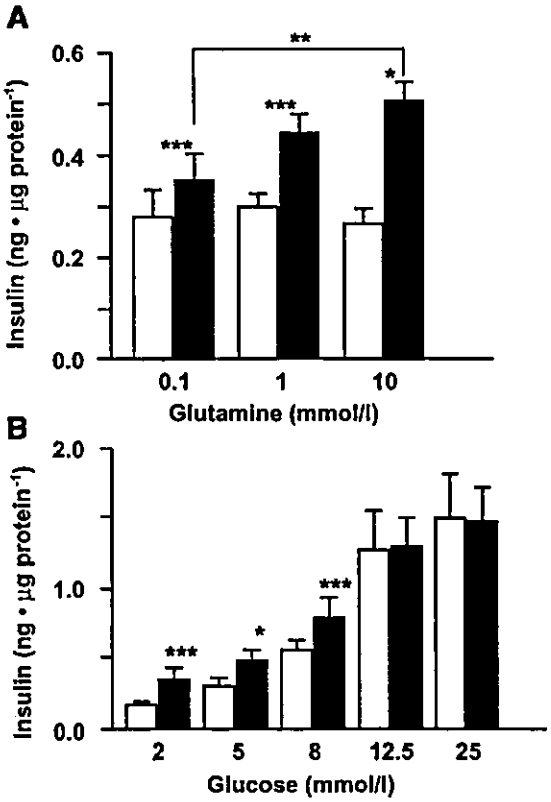

Fig. 3. Glutamine- and glucose-stimulated insulin secretion. *A*: glutamine-stimulated insulin secretion. After a 30-min preincubation in the buffer with 5 mmol/l glucose and without glutamine, pancreatic islets overexpressing GDH266C (Islets-GDH266C; filled bar) and islets overexpressing enhanced green fluorescent protein (Islets-eGFP; open bar) were incubated in the presence of various concentrations of glutamine (without glucose) for 30 min, and insulin released into the incubation buffer was measured. Each assay was performed using 10–30 islets, and values are means ± SE of 3–7 experiments. $^{*}P < 0.01$ and $^{***}P < 0.05$ for comparison between Islets-GDH266C and Islets-eGFP. $^{**}P < 0.02$ for comparison between 0.1 and 10 mmol/l glutamine (Islets-GDH266C) (paired Student's *t*-tests). *B*: glucose-stimulated insulin secretion. After preincubation, Islets-GDH266C (filled bar) and Islets-eGFP (open bar) were incubated in the presence of various concentrations of glucose for 30 min, and insulin released into the incubation buffer was measured. Each assay was performed using 10–30 islets, and values are means ± SE of 6–16 experiments. $^{*}P < 0.01$ and $^{***}P < 0.05$ for comparison between Islets-GDH266C and Islets-eGFP (paired Student's *t*-tests).

and intracellular glutamate content was lower (Fig. 1*B*) in MIN6–266C cells. This observation is consistent with the hypothesis that elevated GDH activity enhances the oxidative deamination of glutamate to α-ketoglutarate to supply TCA cycle substrates (18, 19). It is noteworthy that, at the basal glucose concentration (5 mmol/l) without glutamine in the medium, exaggerated insulin secretion was also associated with enhanced glutamine oxidation, and a decrease in the intracellular glutamate content reflected utilization of the substrate. At this glucose concentration, glutamine (or glutamate) from the intracellular pool would likely be utilized as a substrate of GDH to fuel the TCA cycle and thereby stimulate insulin secretion. At a higher glucose concentration (25 mmol/l), glutamine oxidation also increased, and the cellular glutamate content was lower in MIN6-GDH266C than in MIN6-lacZ cells, although insulin secretion did not differ. Under these conditions, the effect of increased glutamate oxidation on insulin secretion was probably undetectable because glucose stimulation was more potent.

Although the MIN6 cell line is one of the best models of native β-cells (13), it is derived from an insulinoma, and insulin-secretory profiles are known to change over several passages (12). Therefore, this cell line may not adequately reflect native β-cells in some respects. Therefore, we wished to confirm the effect of unregulated elevation of GDH activity on insulin secretion in a more physiological model: isolated rat pancreatic islets. Islets-GDH266C secreted insulin in response to glutamine in a dose-dependent manner (Fig. 3*A*). More importantly, in Islets-GDH266C, insulin secretion was also significantly enhanced at low glucose concentrations (2–8 mmol/l) compared with control Islets-eGFP (Fig. 3*B*), just as we observed in MIN6-GDH266C cells (22). Recently, Kelly et al. (5) reported an H454Y-GDH transgenic mouse. In this animal model, an HI/HA syndrome patient-derived mutant, H454Y-GDH, the activity of which was not inhibited by GTP, was specifically expressed in β-cells. Random blood glucose concentrations were lower than in control mice, and amino acid- and leucine-stimulated insulin secretions from perifused islets were markedly enhanced in these mice. Although glucose-stimulated insulin secretion was reported to be similar to that of control mouse islets, detailed data, including basal insulin secretion at low glucose concentrations, have not been presented. Because basal GDH activity was more than 100 times higher than that in control islets in our model (Table 1), the enhancement of basal insulin secretion might have been more prominent in our model than in the transgenic mouse model.

Physiologically, GDH is an important regulator of glutaminolysis (glutamine oxidation), which may contribute to the interprandial basal insulin secretion (2, 5). Glutaminolysis is regulated by allosteric regulation of GDH with amino acids such as leucine, isoleucine, and methionine. In addition, it is also precisely regulated by glucose metabolism through changes in concentrations of other important allosteric regulators of GDH, GTP, ATP, and ADP. According to this hypothesis, at glucose concentrations near or below its threshold to stimulate insulin secretion (5 mmol/l), GDH is activated by a decrease in the GTP/ADP ratio and drives basal insulin secretion, at least in part (2, 5). Insulin-secretory profiles of MIN6-GDH266C cells and Islets-GDH266C are in agreement with this hypothesis. Constitutively activated GDH rendered the cells responsive to glutamine in insulin secretion in the absence of luecine and enhanced insulin secretion at low glucose concentrations. Furthermore, they would be reflected in the fasting and protein meal-induced hyperinsulinemic hypoglycemia in patients with HI/HA syndrome, although in patients' β-cells elevation of GDH activity at low glucose concentrations would be modest compared with that in MIN6-GDH266C cells and in Islets-GDH266C. On the other hand, in our previous and present studies, glucose-stimulated insulin secretion was not enhanced in either MIN6-GDH266C cells (22) or Islets-GDH266C (Fig. 3*B*). On the basis of the insulin secretion profiles and glutamate metabolism, our data do not support the hypothesis that glutamate, derived from the reverse GDH reaction (flux from α-ketoglutarate to glutamate), is a second messenger of glucose-stimulated insulin secretion (1, 2, 5, 8, 9), although we neither measured the flux directly nor tested

American Journal of Physiology – Endocrinology and Metabolism

the messenger action of glutamate in glucose-stimulated insulin secretion, and therefore the messenger role of glutamate is not completely excluded.

This is the first study, to our knowledge, in which insulin secretion and glutamate metabolism were analyzed simultaneously under conditions of direct and constitutive cellular GDH activity elevation. Our results illustrate the importance of GDH in amino acid-stimulated insulin secretion and possible contribution to the regulation of basal insulin secretion. Furthermore, we have provided additional evidence that, at least under our experimental conditions, the metabolic flux through GDH is in the direction of α-ketoglutarate production in pancreatic β-cells. No evidence was obtained to suggest that glutamate produced by the reverse GDH reaction enhanced insulin secretion.

ACKNOWLEDGMENTS

We thank Prof. Jun-ichi Miyazaki, Osaka University, Japan, for providing us with MIN6 cells. We are grateful to Atsuko Tanimura, Yukari Kora-Miura, and Mayumi Kaneko for expert technical assistance.

GRANTS

This study was supported in part by Grants-in-Aid for Creative Scientific Research (10NP0201 to Y. Oka) and for Scientific Research (14370338 to Y. Tanizawa) from the Ministry of Education, Culture, Sports, Science and Technology of Japan.

REFERENCES

1. **Bertrand G, Ishiyama N, Nenquin M, Ravier MA, and Henquin JC.** The elevation of glutamate content and the amplification of insulin secretion in glucose-stimulated pancreatic islets are not causally related. *J Biol Chem* 277: 32883–32891, 2002.
2. **Gao ZY, Li G, Najafi H, Wolf BA, and Matschinsky FM.** Glucose regulation of glutaminolysis and its role in insulin secretion. *Diabetes* 48: 1535–1542, 1999.
3. **Godel H, Graser T, Foldi P, Pfaender P, and Furst P.** Measurement of free amino acids in human biological fluids by high-performance liquid chromatography. *J Chromatogr* 297: 49–61, 1984.
4. **Hoy M, Maechler P, Efanov AM, Wollheim CB, Berggren PO, and Gromada J.** Increase in cellular glutamate levels stimulates exocytosis in pancreatic beta-cells. *FEBS Lett* 531: 199–203, 2002.
5. **Kelly A, Li C, Gao Z, Stanley CA, and Matschinsky FM.** Glutaminolysis and insulin secretion: from bedside to bench and back. *Diabetes* 51, *Suppl* 3: S421–S426, 2002.
6. **Lacy PE and Kostianovsky M.** Method for the isolation of intact islets of Langerhans from the rat pancreas. *Diabetes* 16: 35–39, 1967.
7. **Liu YJ, Cheng H, Drought H, MacDonald MJ, Sharp GW, and Straub SG.** Activation of the K_{ATP} channel-independent signaling pathway by the nonhydrolyzable analog of leucine, BCH. *Am J Physiol Endocrinol Metab* 285: E380–E389, 2003.
8. **MacDonald MJ and Fahien LA.** Glutamate is not a messenger in insulin secretion. *J Biol Chem* 275: 34025–34027, 2000.
9. **MacMullen C, Fang J, Hsu BY, Kelly A, de Lonlay-Debeney P, Saudubray JM, Ganguly A, Smith TJ, and Stanley CA.** Hyperinsulinism/hyperammonemia syndrome in children with regulatory mutations in the inhibitory guanosine triphosphate-binding domain of glutamate dehydrogenase. *J Clin Endocrinol Metab* 86: 1782–1787, 2001.
10. **Maechler P, Gjinovci A, and Wollheim CB.** Implication of glutamate in the kinetics of insulin secretion in rat and mouse perfused pancreas. *Diabetes* 51, *Suppl* 1: S99–S102, 2002.
11. **Maechler P and Wollheim CB.** Mitochondrial glutamate acts as a messenger in glucose-induced insulin exocytosis. *Nature* 402: 685–689, 1999.
12. **Minami K, Yano H, Miki T, Nagashima K, Wang CZ, Tanaka H, Miyazaki JI, and Seino S.** Insulin secretion and differential gene expression in glucose-responsive and -unresponsive MIN6 sublines. *Am J Physiol Endocrinol Metab* 279: E773–E781, 2000.
13. **Miyazaki J, Araki K, Yamato E, Ikegami H, Asano T, Shibasaki Y, Oka Y, and Yamamura K.** Establishment of a pancreatic beta cell line that retains glucose-inducible insulin secretion: special reference to expression of glucose transporter isoforms. *Endocrinology* 127: 126–132, 1990.
14. **Mizuguchi H and Kay MA.** Efficient construction of a recombinant adenovirus vector by an improved in vitro ligation method. *Hum Gene Ther* 9: 2577–2583, 1998.
15. **Mizuguchi H and Kay MA.** A simple method for constructing E1- and E1/E4-deleted recombinant adenoviral vectors. *Hum Gene Ther* 10: 2013–2017, 1999.
16. **Peterson PE and Smith TJ.** The structure of bovine glutamate dehydrogenase provides insights into the mechanism of allostery. *Structure Fold Des* 7: 769–782, 1999.
17. **Rubi B, Ishihara H, Hegardt FG, Wollheim CB, and Maechler P.** GAD65-mediated glutamate decarboxylation reduces glucose-stimulated insulin secretion in pancreatic beta cells. *J Biol Chem* 276: 36391–36396, 2001.
18. **Sener A and Malaisse WJ.** L-Leucine and a nonmetabolized analogue activate pancreatic islet glutamate dehydrogenase. *Nature* 288: 187–189, 1980.
19. **Sener A, Malaisse-Lagae F, and Malaisse WJ.** Stimulation of pancreatic islet metabolism and insulin release by a nonmetabolizable amino acid. *Proc Natl Acad Sci USA* 78: 5460–5464, 1981.
20. **Stanley CA, Fang J, Kutyna K, Hsu BY, Ming JE, Glaser B, and Poncz M.** Molecular basis and characterization of the hyperinsulinism/hyperammonemia syndrome: predominance of mutations in exons 11 and 12 of the glutamate dehydrogenase gene. HI/HA Contributing Investigators. *Diabetes* 49: 667–673, 2000.
21. **Stanley CA, Lieu YK, Hsu BY, Burlina AB, Greenberg CR, Hopwood NJ, Perlman K, Rich BH, Zammarchi E, and Poncz M.** Hyperinsulinism and hyperammonemia in infants with regulatory mutations of the glutamate dehydrogenase gene. *N Engl J Med* 338: 1352–1357, 1998.
22. **Tanizawa Y, Nakai K, Sasaki T, Anno T, Ohta Y, Inoue H, Matsuo K, Koga M, Furukawa S, and Oka Y.** Unregulated elevation of glutamate dehydrogenase activity induces glutamine-stimulated insulin secretion: identification and characterization of a GLUD1 gene mutation and insulin secretion studies with MIN6 cells overexpressing the mutant glutamate dehydrogenase. *Diabetes* 51: 712–717, 2002.
23. **Tanizawa Y, Ohta Y, Nomiyama J, Matsuda K, Tanabe K, Inoue H, Matsutani A, Okuya S, and Oka Y.** Overexpression of dominant negative mutant hepatocyte nuclear factor (HNF)-1alpha inhibits arginine-induced insulin secretion in MIN6 cells. *Diabetologia* 42: 887–891, 1999.
24. **Ueda K, Tanizawa Y, Ishihara H, Kizuki N, Ohta Y, Matsutani A, and Oka Y.** Overexpression of mitochondrial FAD-linked glycerol-3-phosphate dehydrogenase does not correct glucose-stimulated insulin secretion from diabetic GK rat pancreatic islets. *Diabetologia* 41: 649–653, 1998.
25. **Weinzimer SA, Stanley CA, Berry GT, Yudkoff M, Tuchman M, and Thornton PS.** A syndrome of congenital hyperinsulinism and hyperammonemia. *J Pediatr* 130: 661–664, 1997.
26. **Wrzeszczynski KO and Colman RF.** Activation of bovine liver glutamate dehydrogenase by covalent reaction of adenosine 5′-O-[S-(4-bromo-2,3-dioxobutyl)thiophosphate] with arginine-459 at an ADP regulatory site. *Biochemistry* 33: 11544–11553, 1994.
27. **Yamada H, Yamamoto A, Yodozawa S, Kozaki S, Takahashi M, Morita M, Michibata H, Furuichi T, Mikoshiba K, and Moriyama Y.** Microvesicle-mediated exocytosis of glutamate is a novel paracrine-like chemical transduction mechanism and inhibits melatonin secretion in rat pinealocytes. *J Pineal Res* 21: 175–191, 1996.
28. **Yamada S, Komatsu M, Sato Y, Yamauchi K, Aizawa T, and Hashizume K.** Glutamate is not a major conveyer of ATP-sensitive K+ channel-independent glucose action in pancreatic islet beta cell. *Endocr J* 48: 391–395, 2001.
29. **Zammarchi E, Filippi L, Novembre E, and Donati MA.** Biochemical evaluation of a patient with a familial form of leucine-sensitive hypoglycemia and concomitant hyperammonemia. *Metabolism* 45: 957–960, 1996.

American Journal of Physiology = Endocrinology and Metabolism

0888-8809/04/$15.00/0
Printed in U.S.A.

Molecular Endocrinology 18(2):339–349
Copyright © 2004 by The Endocrine Society
doi: 10.1210/me.2003-0089

Carboxy Terminus of Glucose Transporter 3 Contains an Apical Membrane Targeting Domain

KOUICHI INUKAI, ANNETTE M. SHEWAN, WENDY S. PASCOE, SHIGEHIRO KATAYAMA, DAVID E. JAMES, AND YOSHITOMO OKA

Fourth Department of Internal Medicine (K.I., S.K.), Saitama Medical School, Saitama 350-0495, Japan; and Division of Molecular Metabolism and Diabetes (Y.O.), Department of Internal Medicine Tohoku University Graduate School of Medicine, Miyagi 980-8574, Japan; Institute for Molecular Bioscience (A.M.S., W.S.P., D.E.J.), University of Queensland, Brisbane 4072, Australia; and Garvan Institute of Medical Research (D.E.J.), St. Vincents Hospital, Sydney 2010, Australia

We previously demonstrated that distinct facilitative glucose transporter isoforms display differential sorting in polarized epithelial cells. In Madin-Darby canine kidney (MDCK) cells, glucose transporter 1 and 2 (GLUT1 and GLUT2) are localized to the basolateral cell surface whereas GLUTs 3 and 5 are targeted to the apical membrane. To explore the molecular mechanisms underlying this asymmetric distribution, we analyzed the targeting of chimeric glucose transporter proteins in MDCK cells. Replacement of the carboxy-terminal cytosolic tail of GLUT1, GLUT2, or GLUT4 with that from GLUT3 resulted in apical targeting. Conversely, a GLUT3 chimera containing the cytosolic carboxy terminus of GLUT2 was sorted to the basolateral membrane. These findings are not attributable to the presence of a basolateral signal in the tails of GLUTs 1, 2, and 4 because the basolateral targeting of GLUT1 was retained in a GLUT1 chimera containing the carboxy terminus of GLUT5. In addition, we were unable to demonstrate the presence of an autonomous basolateral sorting signal in the GLUT1 tail using the low-density lipoprotein receptor as a reporter. By examining the targeting of a series of more defined GLUT1/3 chimeras, we found evidence of an apical targeting signal involving residues 473–484 (DRSGKDGVMEMN) in the carboxy tail. We conclude that the targeting of GLUT3 to the apical cell surface in MDCK cells is regulated by a unique cytosolic sorting motif. (*Molecular Endocrinology* 18: 339–349, 2004)

THE DELIVERY SYSTEM for the targeting of membrane proteins to different cell surfaces in polarized cells has been a subject of considerable interest. Many studies have concentrated on identifying the determinants of basolateral and apical sorting signals at the molecular level (1, 2). A number of basolateral sorting signals described to date have been found to reside in the cytoplasmic domain of membrane proteins (3, 4). Most belong to two classes characterized by either a critical tyrosine-containing motif (YXXØ) (5) or a dileucine or leucine residue adjacent to another bulky hydrophobic amino acid (a.a.) (6, 7). These signals have been demonstrated to associate with adaptor protein 1 (8) and adaptor protein 2 (9, 10), which regulate clathrin assembly at the trans-Golgi network and the plasma membrane, respectively. These signals appear to mediate both efficient delivery to the basolateral membrane and endocytic recycling. Conversely, most of the apical signals that have been characterized to date are found in luminal or transmembrane domains. Although relatively little is known about apical sorting signals, both N-linked (11, 12) and O-linked glycosylation (13, 14) have been shown to play an important role.

Facilitative hexose transporters constitute a family of integral membrane proteins that mediate the transport of sugars across cellular membranes (15). These isoforms share a high level of a.a. sequence homology, and their predicted three-dimensional structure is conserved. Considerable evidence suggests that they contain 12 transmembrane domains with both the N and C termini located on the cytosolic side (15). Despite these similarities, major differences in intracellular trafficking have been noted between individual GLUTs. These differences are best demonstrated in polarized cell types in which different transporters have been localized to discrete surfaces. Glucose transporter 1 and 2 (GLUT1 and GLUT2) are principally found on the basolateral surface in epithelial cells whereas GLUT3 and GLUT5 are mainly targeted to the apical domain (16–19). Similar results are obtained when these transporter isoforms are transfected into Madin-Darby canine kidney (MDCK) cells indicating that this is a universal feature of these proteins that can be recapitulated in a heterologous system (20). These results also demonstrate that MDCK cells provide a useful model for studying the vectorial membrane trafficking of facilitative hexose transporters.

Abbreviations: a.a., Amino acid(s); GLUT, glucose transporter; LDL-R, low-density lipoprotein receptor; MDCK, Madin-Darby canine kidney.

***Molecular Endocrinology* is published monthly by The Endocrine Society (http://www.endo-society.org), the foremost professional society serving the endocrine community.**

The asymmetric distribution of GLUTs in polarized cell types has physiological relevance. For example, with respect to the intestinal absorption of fructose, the apically targeted GLUT5 exhibits a high affinity for fructose [low Michaelis-Menten constant (K_m)] (21), whereas the basolaterally targeted GLUT2 exhibits a high V_{max} for fructose (22). Hence, these two facilitative transporters cooperate to achieve efficient absorption of fructose across the gut epithelium.

The molecular mechanisms by which GLUTs are differentially targeted in polarized cells remain to be clarified. Therefore, we attempted to characterize the structural determinants of GLUTs required for this differential targeting. We have expressed a panel of chimeric transporters utilizing various portions of GLUTs 1–5 in MDCK cells and assessed their differential distribution. Our data show that the carboxy-terminal tail of human (h)GLUT3 contains a dominant apical sorting signal that is capable of rerouting both GLUT1 and GLUT2 from the basolateral to the apical cell surface in MDCK cells.

RESULTS

Expression and Analysis of GLUT1/3 Chimeras in MDCK Cells

To clarify the molecular basis for the differential targeting of GLUTs in polarized epithelial cells, we undertook a chimeric strategy whereby different portions of a basolateral transporter and an apical transporter were spliced together and expressed in MDCK cells. Initially, we focused on hGLUT1 and hGLUT3, which are targeted to the basolateral and apical cell surfaces, respectively, in MDCK cells (20). MDCK cells express GLUT1 endogenously but not GLUT3 (20). Initially, we studied the targeting of recombinant hGLUT1 when overexpressed in MDCK cells. Stable cell lines were selected and screened for hGLUT1 expression using a monoclonal antibody that is specific for hGLUT1 (23). This antibody recognizes an epitope in the central loop of hGLUT1 and provides a useful tool for comparing relative expression levels between individual constructs and clones. To verify that this expression system did not result in marked overexpression, we analyzed the glucose transport activities of these clones. In wild-type cells, we observed glucose transport rates of 0.77 ± 0.16 nmol/mg·min and 0.04 ± 0.06 nmol/mg·min across the basolateral and apical membranes, respectively (n = 5, mean ± SD). The glucose transport rates across the basolateral membranes in GLUT1-expressing cell lines were increased at most by 1.5-fold as compared with that observed in wild-type cells. Moreover, we did not observe a significant change in apical transport in clones expressing GLUT1 at this expression level. On the other hand, in clones expressing GLUT3 over a broad range of expression levels, we observed a highly significant increase in transport across the apical membrane (0.56 ± 0.10 nmol/mg·min). Thus, these data provide a good indication that we have performed our studies using nonsaturating expression levels of recombinant transporters. As shown in Fig. 1C (*left upper panel*), at this level of expression the targeting of hGLUT1 was restricted to the basolateral surface as was the case for the endogenous protein. Also shown in Fig. 1C (*right upper panel*) is the distribution of hGLUT3 expressed in MDCK cells. Consistent with our previous findings (20), this protein was highly enriched at the apical cell surface. Whereas these transporters localize to either basolateral or apical membranes, intracellular labeling is also evident. Our focus in this study was the contribution of the cytosolic carboxy terminus to domain-specific cell surface localization and as such we did not characterize the intracellular vesicular compartments through which these chimeras traffic.

The above data provided the basis for our initial studies using hGLUT1/3 chimeras expressed in MDCK cells. We first designed two GLUT1/3 chimeras comprised of different portions of both proteins: hGLUT1/3CT290 contains the N-terminal half of hGLUT1 and the C-terminal half of GLUT3; and hGLUT1/3CT36 is comprised of hGLUT1 in which the carboxy-terminal tail (32 a.a.) has been replaced with that of hGLUT3 (36 a.a.). A scheme of these and other constructs is shown in Fig. 1A. As was the case for all of the constructs described in this study, we selected at least 12 different stable cell lines expressing the recombinant protein of interest and performed detailed analyses on at least three to four different clones for each construct covering a range of expression levels. The targeting of endogenous GLUT1, as well as inulin exclusion, was analyzed in each clone to verify polarity at the time of study (data not shown). Figure 1B shows a Western blot of cell lysates from cells expressing either full-length GLUT3 or the relevant chimeras using an antibody raised against the C-terminal domain of hGLUT3. This antibody did not detect a specific signal in nontransfected MDCK cells, but clearly detected the exogenous hGLUT3 epitope. The chimeras yielded proteins of the appropriate molecular size, *i.e.* similar to that observed for full-length GLUT3. Figure 1C shows the immunolocalization of the hGLUT1/3CT290 (*left lower panel*) and hGLUT1/3CT36 (*right lower panel*) chimeras in MDCK cells as compared with both GLUT1 and GLUT3. Both chimeras were concentrated on the apical domain, similar to the targeting observed for the full-length GLUT3 protein. We also observed labeling of intracellular structures (Fig. 1). This is consistent with our previous studies in which even GLUT1, which is highly concentrated on the basolateral surface (Fig. 1), was also found in intracellular vesicles in MDCK cells (20). These results suggest that the carboxy tails of these transporter proteins determine basolateral *vs.* apical delivery.

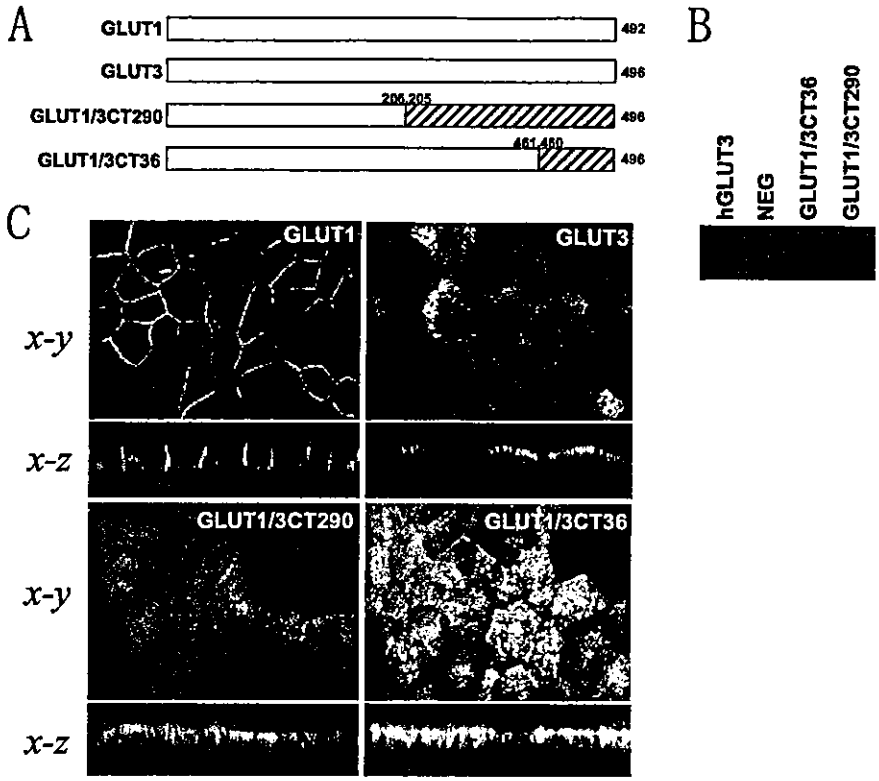

Fig. 1. Immunofluorescence Localizations of GLUT1 and GLUT3 and Their Chimeric GLUTs

A, A diagrammatic representation of the constructs used in these studies is shown. B, Total membrane samples (15 μg) prepared from MDCK cells expressing the indicated proteins were subjected to SDS-PAGE and immunoblotting with an antibody raised against the C-terminal domain of GLUT3. NEG refers to a sample prepared in parallel from parental MDCK cells. Immunoblot data identical to those presented for parental membranes were obtained from nonexpressing but G418-resistant MDCK clones. C, MDCK cells expressing the indicated proteins were plated on glass coverslips, and immunofluorescence was performed as previously described (20). Exogenous transporters were detected using an antibody raised against a short peptide derived from the intracellular loop of hGLUT1 (GLUT1) and an antibody raised against the C-terminal domain of GLUT3 (GLUT3, GLUT1/3CT290, and GLUT1/3CT36). Confocal images were generated using a Zeiss Axiophot fluorescent microscope and a Bio-Rad MRC600 laser scanning head.

Expression of a Low-Density Lipoprotein Receptor (LDL-R)/GLUT1 Chimera in MDCK Cells

It was shown previously that the cytoplasmic tail of the LDL-R possesses two tyrosine-dependent basolateral targeting signals (24, 25). Deletion of these residues resulted in rerouting of the LDL-R to the apical cell surface (24). To determine whether the GLUT1 carboxy tail possesses a basolateral sorting signal, we studied the trafficking of an LDL-R chimera containing the carboxy tail of GLUT1 (LDL-R/G1CT24), in MDCK cells. Several clones expressing the full-length LDL-R and the chimeras were obtained and grown on transwell filters. Trafficking of these proteins was analyzed using a cell surface biotinylation assay (Fig. 2). In agreement with previous studies (24), the wild-type LDL-R was almost entirely targeted to the basolateral membrane, whereas more than 85% of mutated LDL-R (CT37Y-A18) was targeted to the apical membrane. When 24 a.a. from the C terminus of GLUT1 were grafted onto CT37Y-A18, a small portion of the apical proteins relocalized to the basolateral membrane, but the majority remained at the apical membrane (Fig. 2C). These findings suggest that the C-terminal tail of GLUT1 does not contain an autonomous basolateral sorting signal. This does not exclude the possibility of a basolateral sorting signal elsewhere in the GLUT1 molecule. In fact, this seems likely given that it is a multispanning membrane protein with at least three major cytosolic domains. It is also conceivable that sorting domains in these more complex molecules are comprised of discontinuous elements found in discrete domains that interact *in vivo*.

Trafficking of a GLUT1/5 Chimera in MDCK Cells

It was shown previously that GLUT5 is targeted to the apical cell surface in polarized epithelial cells and that apical targeting is regulated via information contained within the central portion of the protein (26). Thus, it is highly unlikely that the C-terminal tail of GLUT5 contains targeting information relevant to trafficking in polarized epithelial cells. Therefore, we reasoned that a GLUT1 chimera containing the C terminus of GLUT5

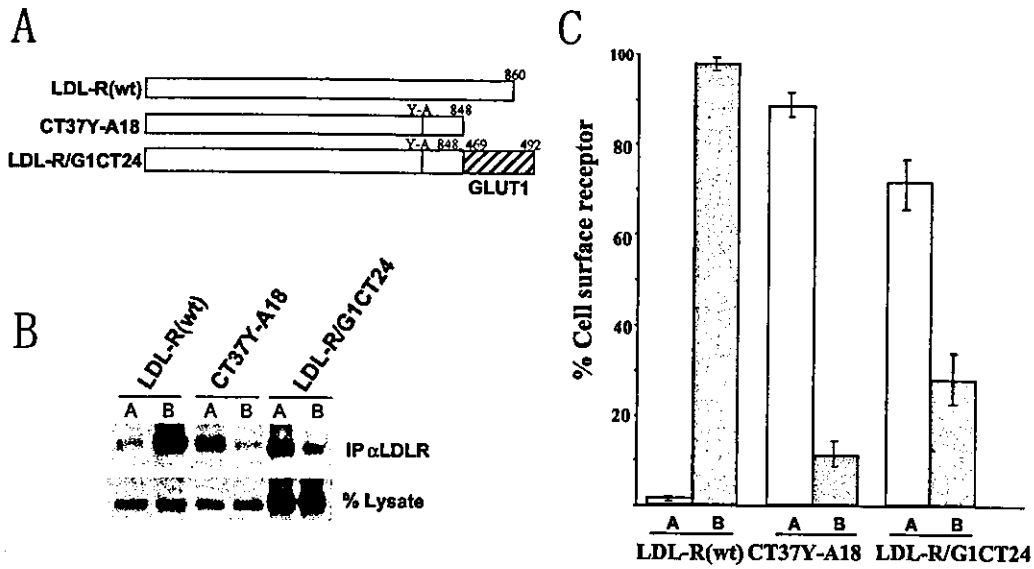

Fig. 2. Cell Surface Distributions of Wild and Mutated LDL-Rs Using Biotinylation Assay

A, A diagrammatic representation of the constructs used in these studies is shown. B, MDCK cells expressing various chimeric proteins were plated onto transwell filters. Apical (A) or basal (B) cell surfaces were incubated in 0.5 mg/ml EZ-link Sulfo-NHS-biotin (Pierce Chemical Co.) for 15 min on ice. Filters were quenched and transferred into lysis buffer, and the solubilized material was cleared by centrifugation. An aliquot of cleared supernatant served as the total expression sample, and the remainder was incubated with streptavidin-agarose to recover biotinylated proteins. Immunoprecipitated proteins were subjected to SDS-PAGE and subsequent Western blot analysis using a polyclonal LDL-R antibody, LB1, with detection performed using goat antirabbit-horseradish peroxidase antibody and enhanced chemiluminescence. C, Values are given as the percent of total cell surface receptors. *Bars* represent the mean ± SD of three independent experiments.

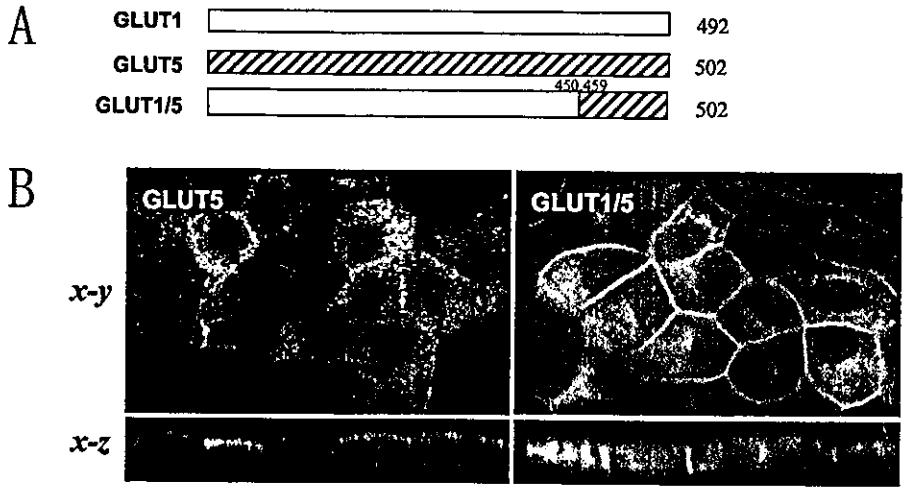

Fig. 3. Immunofluorescence Localizations of GLUT5 and GLUT1/5 Chimeric GLUTs

A, Scheme of the constructs generated for this analysis. B, MDCK cells expressing the indicated proteins were plated onto flamed, glass coverslips and incubated for 5 d to enable tight junction formation and establishment of polarity. Cells were fixed and the domain-specific localizations of exogenous GLUT5 and the GLUT1/5 chimera were assessed by immunofluorescent microscopy using an antibody raised against the C-terminal domain of GLUT5. The GLUT1/5 chimera consists of residues 1–450 of hGLUT1 joined in frame to residues 459–502 of GLUT5.

should provide a useful tool for the present studies. If this chimera targets to the apical cell surface, this will provide definitive proof that the GLUT1 tail contains a basolateral sorting motif. This chimera was expressed in MDCK cells and localized by immunofluorescence microscopy. As shown in Fig. 3, whereas full-length GLUT5 was targeted to the apical surface, the GLUT1/5 chimera was found almost exclusively on the basolateral membrane. In combination with the studies described above, these data strongly indicate that the C-terminal tail of GLUT1 does not contain a basolateral targeting motif.

Expression and Analysis of GLUT2/3 Chimeras in MDCK Cells

To further investigate the apical sorting signal in the C terminus of GLUT3, we undertook an analysis of a panel of chimeras based on hGLUT2 and hGLUT3. Like GLUT1, GLUT2 is targeted to the basolateral cell surface in MDCK cells (20). Initially, we analyzed the targeting of two chimeras, which contained reciprocal portions of GLUT2 and 3. The first, designated GLUT2/3, comprised hGLUT2 up to the end of the last transmembrane domain followed by the cytosolic C-terminal tail of hGLUT3. The second chimera, hGLUT3/2, comprised hGLUT3 up to and including the last transmembrane domain followed by the cytosolic tail of hGLUT2 (Fig. 4A). Both chimeras produced protein products of the correct molecular size when transfected into MDCK cells (data not shown). Confocal immunofluorescence microscopy was used to analyze the targeting of both chimeras in MDCK cells. As shown in Fig. 4B, GLUT2/3 (*left lower panel*) was targeted to the apical membrane and GLUT3/2 (*right lower panel*) to the basolateral membrane. These results support the conclusion that the cytoplasmic carboxy tail of GLUT3 possesses an autonomous apical targeting motif.

Expression and Analysis of GLUT4/3 Chimeras in MDCK Cells

We have previously shown that a chimera composed of the full-length GLUT4 protein and the last 12 a.a. of hGLUT3 appended to the C terminus of GLUT4, when expressed in adipocytes, behaves indistinguishably from GLUT4 (27). This chimera, termed GLUT4/3_{tag}, was expressed in MDCK cells and found to be targeted to intracellular membranes (Fig. 5C, *left panel*) in a manner similar to that previously described for the wild-type GLUT4 protein (20). The intracellular sequestration of GLUT4 is controlled, in part, by an aromatic a.a.-based signal (FQQI) in the cytosolic N terminus of the protein (28). Phenylalanine at position 5 was mutated to alanine in this GLUT4/3_{tag} chimera and expressed in MDCK cells. Localization studies indicated that some GLUT4/3_{tag}F5A was targeted to the basolateral cell surface, whereas others stayed in an intra-

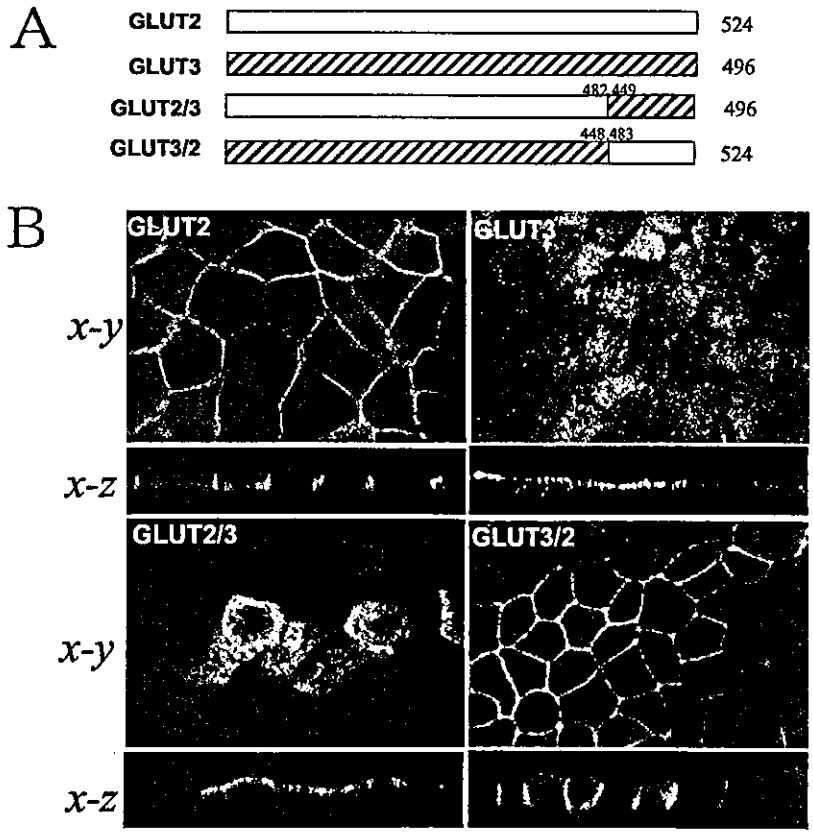

Fig. 4. Immunofluorescence Localizations of GLUT2, GLUT3, and Their Chimeric GLUTs

A, The GLUT2, GLUT3, and the two chimeras generated are represented in this *line drawing*. The chimeras consist of either GLUT2 or 3 up to and including the 12th transmembrane domain of each GLUT with the opposite C-terminal domain fused in frame, generating GLUT2/3 and GLUT3/2. B, At least 4 d before the immunofluorescence study depicted here, MDCK cells expressing the various proteins, as indicated, were plated onto coverslips. The proteins of interest were detected utilizing either an antibody raised against the C-terminal domain of GLUT2 (GLUT2 and GLUT3/2) or an antibody raised against the C-terminal domain of GLUT3 (GLUT3, GLUT2/3). Confocal images were collected and representative images are shown.

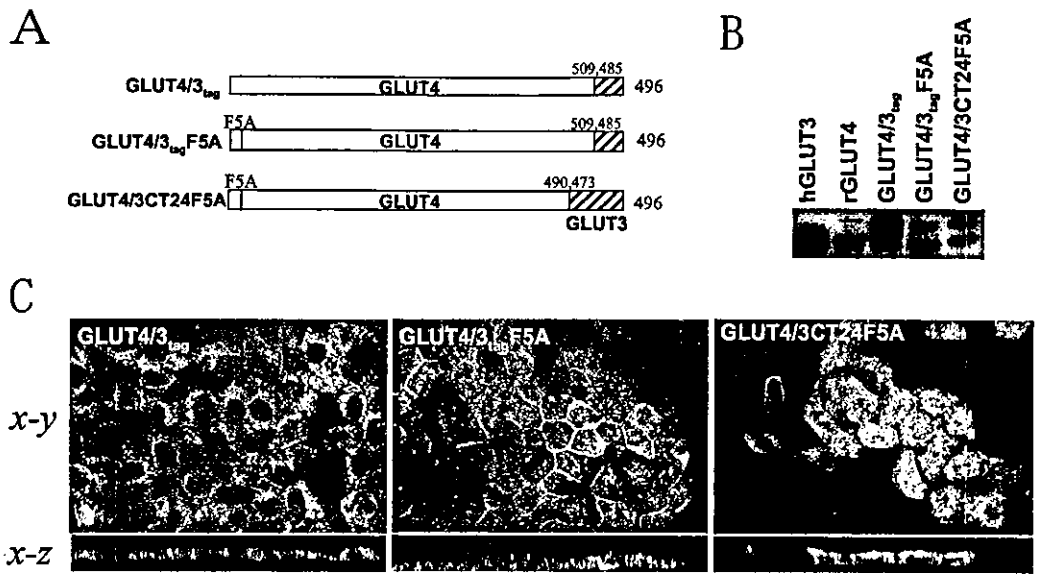

Fig. 5. Immunofluorescence Localizations of GLUT4 and GLUT4/3 Chimeric GLUTs

A, The cDNAs generated for this study and used to transfect MDCK cells are depicted here. As shown, all molecules bear the GLUT3 epitope tag at the extreme carboxy terminus with the Phe5 of GLUT4 mutated to Ala in both GLUT4/3_{tag}F5A and GLUT4/3CT24F5A. B, Western blot analysis of total membrane samples prepared from MDCK cells. Recombinant GLUTs were detected with an anti-GLUT3 antibody. C, MDCK cells expressing GLUT4/3_{tag}, GLUT4/3_{tag}F5A, or GLUT4/3CT24F5A were plated at confluence and allowed to polarize over 5 d. The cellular localization of each of these proteins was assessed by confocal immunofluorescence microscopy using an antibody raised against the GLUT3 carboxy-terminal 12 residues. Representative images are presented.

cellular compartment (Fig. 5C, *middle panel*). Conversely, the chimera GLUT4/3CT24F5A composed of GLUT4 and the cytosolic C-terminal tail of GLUT3 and possessing the Phe5 to Ala mutation was targeted apically (Fig. 5C, *right panel*). Collectively, these data show that the GLUT3 tail possesses an apical targeting signal that does not include the C-terminal 12 a.a.

Further Analysis of GLUT1/3 Chimeras in MDCK Cells

To further define the composition of the apical targeting signal, we examined the targeting of a panel of GLUT1/3 chimeras comprising different portions of the C terminus of GLUT3. Consistent with the data described above (Fig. 5), a chimera in which the last seven a.a. of GLUT1 were replaced with the last 13 a.a. of hGLUT3 (GLUT1/3CT13) was targeted to the basolateral cell surface (Fig. 6C, *middle lower panel*). Intriguingly, addition of a further six a.a. from hGLUT3 (GLUT1/3CT19) resulted in a significant increase in apical targeting although some basolateral targeting was still evident (Fig. 6C, *left lower panel*). However, addition of a further five a.a. from GLUT3 to generate the chimera GLUT1/3CT24 resulted in predominantly apical targeting with little evidence of basolateral localization (Fig. 6C, *right upper panel*). To verify these data, we performed vectorial biotinylation as described above and found that GLUT1/3CT19 was targeted predominantly to the apical side whereas GLUT1/3CT13 was targeted primarily to the basolateral side (Fig. 6D), consistent with our immunofluorescence studies.

As shown in Fig. 6C, expressed GLUT1 occasionally exhibits apparent apical staining in addition to the basolateral staining in immunohistochemical analysis. However, this does reflect, not mixed labeling to different surface domains, but rather both basolateral and intracellular labeling. When the GLUTs reside intracellularly, the outlines of cell nuclei can be seen clearly in x-y images. In contrast, when they localize in apical membranes, the outlines can barely be visualized. When GLUT1s are expressed (Fig. 6C, *left upper panel*), the staining pattern appears to be mixed, similar to those of GLUT1/5 (Fig. 3B) and GLUT3/2 (Fig. 4B). However, this expressed GLUT1 was proved to be located exclusively in the basolateral membrane by biotinylation experiments (Fig. 6D).

DISCUSSION

In the present study, we obtained evidence that the cytosolic carboxy-terminal tail of hGLUT3 contains a targeting motif capable of directing the trafficking of GLUTs 1, 2, and 4 to the apical cell surface in MDCK cells. By examining the targeting of a series of more defined GLUT1/3 chimeras, we found evidence for the presence of an apical targeting signal involving residues 473–484 (DRSGKDGVMEMN) in the carboxy tail. The finding of special interest is that chimeras con-

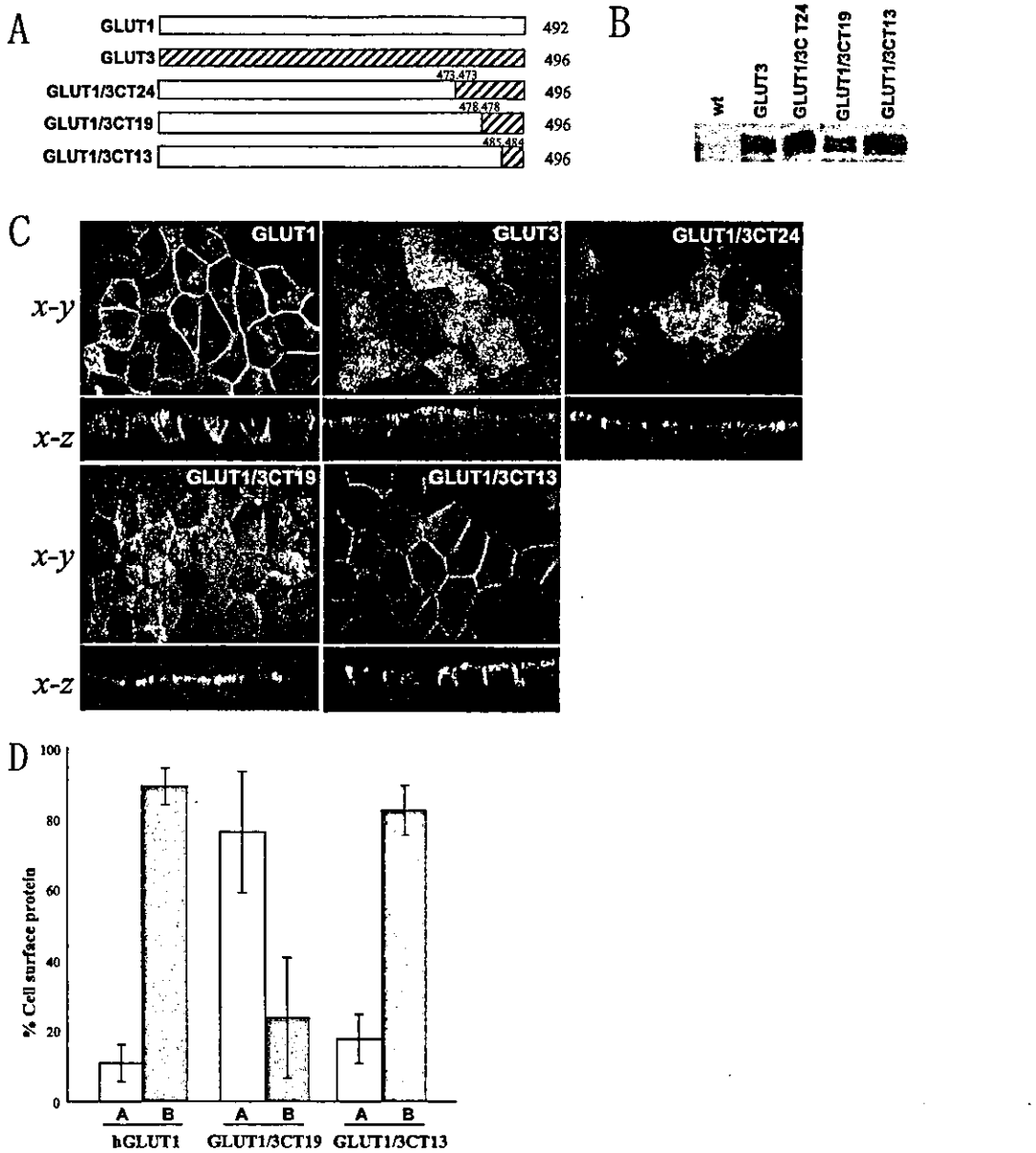

Fig. 6. Immunofluorescence Localizations of GLUT1, GLUT3, and Their Chimeric GLUTs

A, Stable MDCK cell lines were generated by transfection with cDNA, as depicted, and selection in G418. GLUT1/3CT24 consists of a.a. 1–473 of GLUT1 and a.a. 473–496 of GLUT3. Similarly, GLUT1/3CT19 and GLUT1/3CT13 were constructed by fusing a.a. 1–478 (CT19) or a.a. 1–485 (CT13) of GLUT1 to a.a. 478–496 (CT19) or a.a. 484–496 (CT13) of GLUT3. B, Membrane samples were prepared and subjected to SDS-PAGE and Western blot analysis to assess expression levels of GLUTs in MDCK cells. Membranes were incubated with an antibody raised against the C-terminal domain of GLUT3. C, MDCK cells were transfected (with cDNA as indicated in panel A) and clones were analyzed by immunofluorescence microscopy to ascertain the domain-specific localization of the recombinant transporters. Cells were fixed, permeabilized, and immunolabeled using an antibody raised against a short peptide derived from the intracellular loop of hGLUT1 (GLUT1) and an antibody raised against the C-terminal domain of GLUT3 (GLUT3, GLUT1/3CT24, GLUT1/3CT19, and GLUT1/3CT13). Confocal images were generated using a Zeiss Axiophot fluorescent microscope and a Bio-Rad MRC600 laser scanning head. D, Cell surface localizations of overexpressed hGLUT1, hGLUT1/3CT19, and hGLUT1/3CT13 were assessed using a domain-specific biotinylation assay. Cells were grown at confluence for 4–5 d on Transwell filters. Apical and basolateral cell surface proteins were biotinylated by addition of 0.5 mg/ml EZ-Link-Sulfo-NHS-Biotin (Pierce Chemical Co.) for 15 min. Biotinylated proteins were recovered and subjected to SDS-PAGE followed by Western blotting with antibodies specific for hGLUT1. Chemiluminescent bands were quantified using a Bio-Rad 600 densitometer, and signals detected were corrected to account for loading differences.

taining the last 12 or 13 a.a. of GLUT3 did not exhibit significant apical targeting, whereas a chimera containing a further seven a.a. from GLUT3 (GLUT1/3CT19) exhibited significant apical targeting. Thus, fine mapping of the C-terminal tail of hGLUT3 has narrowed the apical sorting information to a small

region encompassing residues DGVMEMN, which corresponds to residues PAGVELN in rodent GLUT3. It is noteworthy that this chimera (GLUT1/3CT19) was partially targeted to the basolateral membrane whereas GLUT1/3CT24, which contained an additional five a.a. from GLUT3, was targeted almost indistinguishably from wild-type GLUT3. To our knowledge, no similar targeting motifs have been reported in other apical membrane proteins, and we have been unable to identify a similar motif in other apical membrane proteins. Most noteworthy is the presence of two conserved hydrophobic residues surrounding an acidic residue in both the rodent (VEL) and human (MEM) sequences. Future studies will be aimed at identifying the roles of these residues.

Based upon our initial studies with GLUT1/3 chimeras (Fig. 1), we hypothesized that the GLUT1 tail contained a basolateral signal that was disrupted in this chimera, resulting in default trafficking to the apical cell surface. However, detailed studies showed that this was not the case and argued in favor of an apical signal in GLUT3. Most notably, the GLUT3 tail facilitated apical targeting when grafted onto GLUT1, 2, or 4, all of which normally recycle via the basolateral cell surface. Thus far, two separate classes of basolateral sorting signals have been identified. These are characterized by either an essential tyrosine residue, or a dileucine motif (5–7). Similar kinds of motifs could not be found in the C termini of either GLUT1 or GLUT2 (Fig. 7). The LGA residues are conserved between GLUT1 and GLUT2 in the C terminus. However, mutating all of these residues did not disrupt the basolateral targeting of GLUT1 (data not shown). We also prepared a GLUT1 mutant missing the last three a.a. because this domain has been shown to act as a binding site for PDZ domain-containing proteins (29, 30). However, the distribution of this truncated GLUT1 was exactly the same as that of wild-type GLUT1 (data not shown). Thus, using this type of approach, we were unable to identify a basolateral targeting domain in the tail of GLUT1. Consistent with this conclusion, the GLUT1 tail did not significantly alter the apical targeting of a tail minus LDL-R, a construct that has been successfully used to map basolateral sorting signals in cytosolic tails (Fig. 2). Moreover, the cytosolic tail of GLUT5, which does not contain a basolateral sorting signal, did not disrupt the targeting of GLUT1 (Fig. 3). Taken together, these studies provide compelling evidence that the C-terminal tail of GLUT3 contains an apical sorting signal. This signal is obviously very dominant, being able to overcome basolateral sorting signals in GLUTs 1, 2, and 4.

It was reported previously that some apical targeting motifs function by selectively partitioning into lipid raft domains in the Golgi (31). Intriguingly, it was reported recently that, in nonpolarized epithelial cells, whereas a substantial portion of GLUT1 was found in detergent-resistant membrane domains, this was not the case for GLUT3 (32). Hence, these data support the notion that GLUT3 is sorted via a non-lipid raft-mediated domain; this is consistent with the present data indicating such a domain to be located in the cytosol, perhaps allowing the transporter to interact with cytosolic targeting machinery. Several other reports have recently found narrowly defined sequences or short peptides in the C-terminal cytoplasmic tails of membrane proteins to have a role in apical targeting (33–37). Among them, multiple autonomous signals for apical targeting in the same protein have been reported (33, 34). These signals include PDZ-interacting domains (35) and β-turn structures (36) as well as less well-defined signals. Taken together, these observations suggest the apical sorting mechanism defined by cytosolic sorting signals to be less well defined than luminal or transmembrane signals, and further work is required to determine whether there is some type of homology among these motifs.

GLUT3 has been shown to undergo specialized targeting in other cell types. It is targeted to the limited membrane of secretory granules in platelets (38) and to the tail of sperm cells (39). Moreover, there is evidence that GLUT3 is targeted to axons in neurons (our unpublished data) and also to neuronal vesicles (40). It will be intriguing to determine whether the cytosolic C terminus is involved in each of these unique trafficking processes, which would imply a common mechanism. Consistent with this, it was previously suggested that similar rules govern the targeting of membrane proteins in epithelial cells and neurons (41).

The identification of this apical targeting signal in the GLUT3 tail may have significant utility in studying the structure/function of sugar transporters in mammalian

```
human GLUT1-KVPETKGRTFDEIASGFRQGGASQSDKTPEEIFHPLGADSQV        492
human GLUT2-KVPETKGKSFEEIAAEFQKKSGSAHRPKAAVEMKFLGATETV       524
mouse GLUT2-KVPETKGKSFEEIAAEFRKKSGSAPPRKAAVQMEFLASSESV       523
human GLUT3-KVPETRGRTFEDITRAFECQAHGADRSGKD--GVMEMNSIEPAKETTTNV    496
mouse GLUT3-KVPETKGRTFEDIARAFECQAH-----SGKGPAGV-ELNSMQPVKETPGNA   493
rat   GLUT3-KVPETKGRTFEDITRAFECQAH-----SGKGSAGV-ELNSMQPVKETPGNA   493
human GLUT4-RVPETRGRTFDQISAAFHRTPSLLEQEVKPSTELEYLGPDEND      509
human GLUT5-IVPETKAKTFIEINQIFTKMNKVSEVYPEKEELKEL----PPVTSEQ  501
rat   GLUT5-VVPETKGRTFVEINQIFAKKNKVSDVYPEKEE-KELNDLPPATREQ   502
```

Fig. 7. Comparison of the Cytoplasmic Tails of Human and Rodent GLUTs

The putative a.a. sequence, which is suggested to have an apical sorting signal, is *underlined*.

cells. A major complication of studying transport kinetics of GLUTs after their expression in mammalian cells is that there is always a very high background due to the presence of endogenous transporters. We previously found that glucose transport across the apical cell surface in MDCK cells is negligible because most of the uptake occurs via the basolateral surface (20). By transplanting the apical signal from GLUT3 onto other transporters it should be feasible to redirect them to the apical surface, as shown here, which should afford ideal conditions for studying transport kinetics in a more appropriate environment.

In conclusion, we have analyzed the asymmetric distribution of facilitative GLUTs by expressing chimeric transporters utilizing various portions of GLUTs (GLUT1–GLUT5) in MDCK cells. Our present data strongly suggest that the apical sorting signal resides in the C-terminal tail of GLUT3.

MATERIALS AND METHODS

cDNA Constructs

Chimeric cDNAs were produced according to previously described methods (42), which allowed us to swap different domains from different transporter isoforms at any desired junction. A hGLUT1 cDNA (23), a hGLUT2 cDNA (42), a hGLUT3 cDNA (27), a hGLUT4 cDNA (28), and a rat GLUT5 cDNA (43) were used as PCR templates. Cytomegalovirus-based expression plasmid pCB6 was generously supplied by Dr. Mellman (4). Fragments prepared by PCR were fully sequenced and observed to have no unexpected mutations. cDNAs encoding wild-type and chimeric GLUTs were ligated into pCB6 vectors.

Cell Culture and Transfection

MDCK cells were cultured in DMEM supplemented with 10% fetal calf serum, 2 mM L-glutamine, 100 U/ml penicillin, and 100 μg/ml streptomycin at 37 C, in 5% CO_2. Lipofectamine reagent, Opti-MEM I, and G-418 (geneticin) were purchased from GIBCO Life Technologies (Eggenstein, Germany). One day before transfection, MDCK cells were trypsinized and seeded onto a 60-mm plastic culture dish at 6 x 10^5cells per dish. The following day, transfection procedures were performed using 30 μl lipofectamine diluted in 300 μl Opti-MEM I (supplemented with 20 mM L-glutamine) and 6 μg GLUT/pCB6 diluted in 300 μl of supplemental Opti-MEM-I/60-mm dish. Cells were incubated in the presence of the lipofectamine-DNA mix for 5 h at 37 C, in 5% CO_2, and then incubated overnight in DMEM-10% fetal calf serum-L-glutamine. Forty-eight hours after transfection, each transfected 60-mm dish was split into three 150-mm dishes and incubated with G-418 (0.8 mg/ml). Colonies resistant to G-418 were isolated after 10–14 d and screened for protein expression by Western blotting.

Western Blotting

To screen for positive expression of the chimera of interest, membrane protein samples (20 μg protein) were subjected to SDS-PAGE employing a 10% resolving gel. Proteins were transferred to a nitrocellulose membrane. Membranes were incubated for 1 h at 37 C with the appropriate primary antibody. After three 10-min washes in PBS-0.1% Tween 20, the membranes were incubated at room temperature for 1 h with a horseradish peroxidase-labeled donkey antirabbit secondary antibody (Amersham Life Science, Little Chalfont, Buckinghamshire, UK) diluted 1:10,000 in PBS-0.2% BSA. After three further washes, labeled proteins were visualized using the enhanced chemiluminescence detection method (Amersham Life Science).

Preparation of Total Membrane Fractions

Total membrane fractions were prepared from MDCK cells after homogenization in 20 mM HEPES, pH 7.4, 1 mM EDTA, 255 mM sucrose buffer containing protease inhibitors (10 μg/ml aprotinin, 10 μg/ml leupeptin, 250 μM phenylmethylsulfonylfluoride) and centrifugation at 50,000 rpm in a Beckman TLA100–3 rotor (Beckman Coulter, Inc., Fullerton, CA) for 60 min. The membrane pellet was resuspended in 20 mM HEPES, pH 7.4, 1 mM EDTA, 255 mM sucrose buffer and stored at −80 C before use.

Protein Assay

The protein concentration of total membrane fractions was determined using the bicinchoninic acid assay (Pierce Chemical Co., Rockford, IL) according to the manufacturer's instructions.

Immunofluorescence Microscopy

Cells were plated at near-confluent density on glass coverslips and fixed 5 d later in 2% paraformaldehyde-PBS for 1 h at room temperature. Polarization was indicated by the presence of domes or blisters in the cultures. Coverslips were washed three times in PBS, and then quenched for 15 min in 0.2% Triton X-100. After an additional three washes in PBS, coverslips were blocked for 30 min in 2% horse serum-PBS and then washed twice in PBS. Primary antibodies were diluted in 0.1% horse serum-PBS, and incubations were carried out at 4 C overnight. Fluorescein isothiocyanate-conjugated antirabbit Ig secondary antibody diluted in 0.1% horse serum-PBS was applied after three 5-min washes in PBS. After a 1-h incubation, at room temperature, coverslips were washed three times in PBS for 5 min each and then mounted in 1% propyl gallate-50% glycerol-PBS. Confocal images were generated with a Zeiss Axiophot microscope (Carl Zeiss, Thornwood, NY) and a Bio-Rad MRC600 confocal laser scanning head (Bio-Rad Laboratories, Inc., Hercules, CA). At least one G-418-resistant clone, which was negative by immunoblotting, served as a negative control for immunofluorescence microscopy.

Cell Surface Biotinylation

Localization of the LDL-R constructs and GLUT1/3 chimeras was assessed utilizing a domain-specific biotinylation assay. Briefly, MDCK cells expressing various chimeric proteins were plated onto transwell filters (Corning, Inc., Corning, NY) and grown for at least 4 d at 37 C and 5% CO_2. To assess the integrity of the monolayer, growth media containing [^{14}C]inulin (0.1 mCi/ml at 1:2000 dilution) were added to the apical chamber and incubated for 1 h. After this incubation, aliquots of medium from both the apical and basal chambers were counted (Coulter Counter, BD, Beckman Coulter, Inc.). Transwells with less than 0.5% transport were used in experiments. Filters were washed three times with ice-cold PBS containing 1 mM $MgCl_2$ and 0.1 mM $CaCl_2$ (PBS+). Apical or basal cell surfaces were incubated with 0.5 mg/ml EZ-link Sulfo-NHS-biotin (Pierce Chemical Co.) for 15 min on ice. This process was repeated, and the free biotin reagent was then quenched by washing with PBS+ containing 50 mM

glycine. Filters were transferred into lysis buffer (1% TX-100, 20 mM HEPES, 1 mM EDTA, 100 mM NaCl, aprotinin 10 μg/ml, leupeptin 10 μg/ml, and phenylmethylsulfonylfluoride 250 μM) for 30 min on ice and vortexed, and solubilized material was cleared by centrifugation at 14,000 rpm at 4 C for 15 min. An aliquot of cleared supernatant served as the total expression sample, and the remainder was incubated with streptavidin-agarose (Sigma Chemical Co., St. Louis, MO) to recover biotinylated proteins. Immunoprecipitated proteins were subjected to SDS-PAGE and subsequent Western blot analysis using either a polyclonal LDL-R antibody, LB1 (gift from Dr. P. Kroon, Department of Biochemistry, University of Queensland), or antibodies specific to hGLUT1 (gift from Dr. G. Lienhard, Department of Biochemistry, Dartmouth Medical School, Hanover, NH). Detection was performed using goat antirabbit-horseradish peroxidase antibody (Amersham Life Science) and enhanced chemiluminescence (SuperSignal, Pierce Chemical Co.).

Acknowledgments

Received March 18, 2003. Accepted October 30, 2003.

Address all correspondence and requests for reprints to: David E. James, Garvan Institute of Medical Research, St. Vincents Hospital, Sydney 2010, Australia. E-mail: d.james@garvan.org.au; or Yoshitomo Oka, Division of Molecular Metabolism and Diabetes, Department of Internal Medicine Tohoku University Graduate School of Medicine, Miyagi 980-8574, Japan. E-mail: oka@int3.med.tohoku.ac.jp.

K.I. and A.M.S. contributed equally to this work and should both be considered first authors.

This work was supported by the Research Council of Australia, of which D.E.J. is a Senior Principal Research Fellow of the National Health and Medical Research Council of Australia. This work was also supported by Grant-in Aid for Scientific Research no. 13470226 (to Y.O.) and Creative Basic Research Grant no. 10NP0201 (to Y.O.) from the Ministry of Education, Culture, Sports, Science, and Technology of Japan.

REFERENCES

1. Matter K, Mellman I 1994 Mechanisms of cell polarity: sorting and transport in epithelial cells. Curr Opin Cell Biol 6:545–554
2. Simon K, Wandinger-Ness A 1990 Polarized sorting in epithelia. Cell 62:207–210
3. Casanova JE, Apodaca G, Mostov KE 1991 An autonomous signal for basolateral sorting in the cytoplasmic domain of the polymeric immunoglobulin receptor. Cell 66:65–75
4. Hunziker W, Harter C, Matter K, Mellman I 1991 Basolateral sorting in MDCK cells requires a distinct cytoplasmic domain determinant. Cell 66:907–920
5. Marks MS, OhnoH, Kirchhausen T, Bonifacino JS 1997 Protein sorting by tyrosine-based signals: adapting to the Ys and wherefores. Trends Cell Biol 7:124–128
6. Pond L, Kuhn LA, Teyton L, Schutze MP, Tainer JA, Jackson MR, Peterson PA 1995 A role for acidic residues in di-leucine motif-based targeting to the endocytic pathway. J Biol Chem 270:19989–19997
7. Sandoval IV, Bakke O 1994 Targeting of membrane proteins to endosomes and lysosomes. Trends Cell Biol 4:292–297
8. Rapoport I, Chen YC, Cupers P, Shoelson S, Kirchhausen T 1998 Dileucine-based sorting signals bind to the β chain of AP-1 at a site distinct and regulated differently from the tyrosine-based motif-binding site. EMBO J 17:2148–2155
9. Rapoport I, Moyazaki M, Boll W, Duckworth B, Cantley LC, Shoelson S, Kirchhausen T 1997 Regulatory interactions In the recognition of tyrosine-based endocytic signals by clathrin AP-2 complexes. EMBO J 16:2240–2250
10. Rodionov DG, Bakke O 1998 Medium chains of adaptor complexes AP-1 and AP-2 recognize leucine-based sorting signals from the invariant chain. J Biol Chem 273: 6005–6008
11. Urban J, Parczyk K, Leutz A, Kayne M, Kondor-Koch C 1987 Constitutive apical secretion of an 80-kD sulfated glycoprotein complex in the polarized epithelial Madin-Darby canine kidney cell line. J Cell Biol 105:2735–2743
12. Kitagawa Y, Sano Y, Ueda M, Higashio K, Narita H, Okano M, Matsumoto S, Sasaki R 1994 N-glycosylation of erythropoietin is critical for apical secretion by Madin-Darby canine kidney cells. Exp Cell Res 213:449–457
13. Jacob R, Alfalah M, Grunberg J, Obendorf M, Naim HY 2000 Structural determinants required for apical sorting of an intestinal brush-border membrane protein. J Biol Chem 275:6566–6572
14. Monlauzeur L, Breuza L, Le Bivic A 1998 Putative O-glycosylation sites and a membrane anchor are necessary for apical delivery of the human neurotrophin receptor in Caco-2 cells. J Biol Chem 273:30263–30270
15. Bell GI, Kayano T, Buse JB, Burant CF, Takeda J, Lin D, Fukumoto H, Seino S 1990 Molecular biology of mammalian glucose transporter. Diabetes Care 13:198–208
16. Thorens B, Cheng ZQ, Brown D, Lodish HF 1990 Liver glucose transporter: a basolateral protein in hepatocytes and intestine and kidney cells. Am J Physiol 259: C279–C285
17. Rand EB, Depaoli AM, Davidson NO, Bell GI, Burant CF 1993 Sequence, tissue distribution, and functional characterization of the rat fructose transporter GLUT5. Am J Physiol 264:G1169–G1176
18. Harris DS, Slot JW, Geuze HJ, James DE 1992 Polarized distribution of glucose transporter isoforms in Caco-2 cells. Proc Natl Acad Sci USA 89:7556–7560
19. Davidson NO, Hausman AML, Ifkovits CA, Buse JB, Gould GW, Burant CF, Bell GI 1992 Human intestinal glucose transporter expression and localization of GLUT5. Am J Physiol 262:C795–C800
20. Pascoe WS, Inukai K, Oka Y, Slot JW, James DE 1996 Differential targeting of facilitative glucose transporter in polarized epithelial cells. Am J Physiol 271:C547–C554
21. Inukai K, Katagiri H, Takata K, Asano T, Anai M, Ishihara H, Nakazaki M, Kikuchi M, Yazaki Y, Oka Y 1995 Characterization of rat GLUT5 and functional analysis of chimeric proteins of GLUT1 glucose transporter and GLUT5 fructose transporter. Endocrinology 136:4850–4857
22. Colville CA, Seatter MJ, Jess TJ, Gould GW, Thomas HM 1993 Kinetic analysis of the liver-type (GLUT2) and brain-type (GLUT3) glucose transporter in *Xenopus* oocytes: substrates specificities and effects of transport inhibitors. Biochem J 290:701–706
23. Davies A, Ciardelli TL, Lienhard GE, Boyle JM, Whetton AD, Baldwin SA 1990 Site-specific antibodies as probes of the topology and function of the human erythrocyte glucose transporter. Biochem J 266:799–808
24. Matter K, Hunziker W, Mellman I 1992 The cytoplasmic domain contains two tyrosine-dependent targeting determinants. Cell 71:741–753
25. Matter K, Whitney JA, Yamamoto EM, Mellman I 1993 Common signals control low density lipoprotein receptor sorting in endosomes and the Golgi complex of MDCK cells. Cell 74:1053–1064
26. Inukai K, Takata K, Asano T, Katagiri H, Ishihara H, Nakazaki M, Fukushima Y, Yazaki Y, Kikuchi M, Oka Y 1997 Targeting of GLUT1–GLUT5 chimeric proteins in the polarized cell line Caco-2. Mol Endocrinol 11:442–449
27. Shewan AM, Marsh BJ, Melvin DR, Martin S, Gould GW, James DE 2000 The cytosolic C-terminus of the glucose transporter GLUT4 contains an acidic cluster endosomal

targeting motif distal to the dileucine signal. Biochem J 350:99–107
28. Piper RC, Tai C, Kulesza P, Pang S, Warnock D, Baenziger J, Slot JW, Geuze HJ, Puri C, James DE 1993 GLUT4 NH2 terminus contains a phenylalanine-based targeting motif that regulates intracellular sequestration. J Cell Biol 121:1221–1232
29. Bunn RC, Jensen MA, Reed BC 1999 Protein interactions with the glucose transporter binding protein GLUT1CBP that provide a link between GLUT1 and the cytoskeleton. Mol Biol Cell 10:819–832
30. Songyang Z, Fanning AS, Fu C, Xu J, Marfatia SM, Chishti AH, Crompton A, Chan AC, Anderson JM, Cantley LC 1997 Recognition of unique carboxy-terminal motifs by distinct PDZ domains. Science 275:73–77
31. Brown D, Rose J 1991 Sorting of GPI-anchored protein to glycolipid-enriched membrane subdomains during transport to the apical cell surface. Cell 68:533–544
32. Sakyo T, Kitagawa T 2002 Differential localization of glucose transporter isoforms in non-polarized mammalian cells: distribution of GLUT1 but not GLUT3 to detergent-resistant membrane domains. Biochim Biophys Acta 1567:165–175
33. Jolimay N, Franck L, Langlois X, Hamon M, Darmon M 2000 Dominant role of the cytosolic C-terminal domain of the rat 5-HT1B receptor in axonal-apical targeting. J Neurosci 20:9111–9118
34. Tugizov S, Maidji E, Xiao J, Zheng Z, Pereira L 1998 Human cytomegalovirus glycoprotein B contains autonomous determinants for vectorial targeting to apical membranes of polarized epithelial cells. J Virol 72: 7374–7386
35. Milewski MI, Mickle, JE, Forrest JK, Stafford DM, Moyer BD, Cheng J, Guggino WB, Stanton BA, Cutting GR 2001 A PDZ-binding motif is essential but not sufficient to localize the C terminus of CFTR to the apical membrane. J Cell Sci 114:719–726
36. Sun AQ, Salkar R, Xu SS, Zeng L, Zhou MM, Suchy FJ 2003 A 14-amino acid sequence with a β-turn structure is required for apical membrane sorting of the rat ileal bile acid transporter. J Biol Chem 278:4000–4009
37. Chuang JZ, Sung CH 1998 The cytoplasmic tail of rhodopsin acts as a novel apical sorting signal in polarized MDCK cells. J Cell Biol 142:1245–1256
38. Heijnen HF, Oorschot V, Sixma JJ, Slot JW, James DE 1997 Thrombin stimulates glucose transport in human platelet via translocation of the glucose transporter GLUT3 from α-granules to the cell surface. J Cell Biol 138:323–330
39. Angulo C, Rauch MC, Droppelmann A, Reyers AM, Slebe JC, Delgado-Lopez F, Guaiquil VH, Vera JC, Concha II 1998 Hexose transporter expression and function in mammalian spermatozoa: cellular localization and transport of hexoses and vitamin C. J Cell Biochem 71: 189–203
40. Thoidis G, Kupriyanova T, Cunningham JM, Chen P, Cadel S, Foulon T, Cohen P, Fine RE, Kandror KV 1999 Glucose transporter GLUT3 is targeted to secretory vesicles in neurons and PC12 cells. J Biol Chem 274: 14062–14066
41. Dotti CG, Simons K 1990 Polarized sorting of viral glycoproteins to the axon and dendrites of hippocampal neurons in culture. Cell 62:63–72
42. Katagiri H, Asano T, Ishihara H, Tsukuda K, Lin JL, Inukai K, Kikuchi M, Yazaki Y, Oka Y 1992 Replacement of intracellular C-terminal domain of GLUT1 glucose transporter with that of GLUT2 increases V_{max} and K_m of transport activity. J Biol Chem 267:22550–22555
43. Inukai K, Asano T, Katagiri H, Ishihara H, Anai M, Fukushima Y, Tsukuda K, Kikuchi M, Yazaki Y, Oka Y 1993 Cloning and increased expression with fructose feeding of rat jejunal GLUT5. Endocrinology 133: 2009–2014

Molecular Endocrinology **is published monthly by The Endocrine Society (http://www.endo-society.org), the foremost professional society serving the endocrine community.**

Available online at www.sciencedirect.com
SCIENCE DIRECT®
Biochemical and Biophysical Research Communications 325 (2004) 250–256
BBRC
www.elsevier.com/locate/ybbrc

Endoplasmic reticulum stress and N-glycosylation modulate expression of WFS1 protein

Suguru Yamaguchi[a], Hisamitsu Ishihara[a,*], Akira Tamura[a], Takahiro Yamada[a], Rui Takahashi[a], Daisuke Takei[a], Hideki Katagiri[b], Yoshitomo Oka[a]

[a] *Division of Molecular Metabolism and Diabetes, Tohoku University Graduate School of Medicine, 2-1 Seiryo-machi, Aoba-ku, Sendai, Miyagi 980-8575, Japan*

[b] *Division of Advanced Therapeutics for Metabolic Diseases, Tohoku University Graduate School of Medicine, 2-1 Seiryo-machi, Aoba-ku, Sendai, Miyagi 980-8575, Japan*

Received 22 September 2004
Available online 22 October 2004

Abstract

Mutations of the *WFS1* gene are responsible for two hereditary diseases, Wolfram syndrome and low frequency sensorineural hearing loss. The WFS1 protein is a glycoprotein located in the endoplasmic reticulum (ER) membrane but its function is poorly understood. Herein we show WFS1 mRNA and protein levels in pancreatic islets to be increased with ER-stress inducers, thapsigargin and dithiothreitol. Another ER-stress inducer, the N-glycosylation inhibitor tunicamycin, also raised WFS1 mRNA but not protein levels. Site-directed mutagenesis showed both Asn-663 and Asn-748 to be N-glycosylated in mouse WFS1 protein. The glycosylation-defective WFS1 protein, in which Asn-663 and Asn-748 had been substituted with aspartate, exhibited an increased protein turnover rate. Consistent with this, the WFS1 protein was more rapidly degraded in the presence of tunicamycin. These data indicate that ER-stress and N-glycosylation play important roles in WFS1 expression and stability, and also suggest regulatory roles for this protein in ER-stress induced cell death.
© 2004 Elsevier Inc. All rights reserved.

Keywords: Wolfram syndrome; Low frequency sensorineural hearing loss; WFSI; ER-stress; N-Glycosylation

The *WFS1* gene, encoding a transmembrane protein of the endoplasmic reticulum (ER) [1], is mutated in two hereditary diseases, autosomal recessive Wolfram syndrome (OMIN:222300) [2,3] and autosomal dominant low frequency sensorineural hearing loss (LFSNHL) (OMIM:600965) [4,5]. The former is also known as DIDMOAD, summarizing the most frequent symptoms; diabetes insipidus, diabetes mellitus, optic atrophy, and deafness. More than 100 mutations of the *WFS1* gene have been identified to date in patients with these diseases [6]. WFS1 protein, also called wolframin, consists of 890 amino acids [2,3] and its homologues are found in several organisms; *Drosophila melanogaster* (CG4917), *Anopheles gambiae* (EBIP3764), *Ciona intestinalis* (Cin.16116), *Fugu rubripes* (SINFRUP82345), and *Xenopus laevis* (Xl.3995). However, these proteins share no homology with known proteins, making it difficult to speculate as to their functions.

We recently established a murine model with a disrupted *wfs1* gene [7]. Mutant mice exhibited impaired glucose homeostasis due to defective insulin secretion in vivo. Studies using isolated islets revealed that mutant islet cells were prone to apoptosis induced by insults which impair ER functions and trigger the so-called unfolded protein response (UPR) [8,9]. Therefore, it was suggested that WFS1 protein plays a role in modulation of apoptotic processes that arise from impairment of ER function [7]. In addition, isolated islets from WFS1-deficient mice exhibited defective insulin

* Corresponding author. Fax: +81 22 717 7612.
E-mail address: ishihara-tky@umin.ac.jp (H. Ishihara).

0006-291X/$ - see front matter © 2004 Elsevier Inc. All rights reserved.
doi:10.1016/j.bbrc.2004.10.017

secretion which was accompanied by decreased calcium responses to glucose. Conversely, wolframin-overexpressing islets showed increased insulin secretion, indicating that wolframin also participates in regulation of stimulus-secretion coupling in insulin exocytosis [7]. It has recently been reported that WFS1 protein/wolframin expression in *Xenopus* oocytes conferred cation channel activity and increased cytosolic calcium levels [10]. This observation is intriguing since intracellular calcium regulation plays important roles in modulating both apoptotic and exocytotic processes. Despite these advancements, however, little is known about the mechanisms by which WFS1 protein actually alters these processes.

To understand the role that WFS1 protein/wolframin plays in the regulation of apoptotic and exocytotic events as well as in other as yet unknown cellular processes, information on the structure and function of this protein must be obtained. The amino acid sequence suggests that WFS1 protein is a multi-membrane spanning protein with hydrophilic amino (N)- and carboxy (C)-terminal regions [2,3]. In addition, biochemical and immunocytochemical analyses showed WFS1 protein to be an ER membrane glycoprotein [1].

In the present studies, we first examined WFS1 protein expression after treatment with agents that trigger UPR. We found WFS1 mRNA and protein levels to be increased by thapsigargin or dithiothreitol (DTT). Treatment with tunicamycin, an inhibitor of N-glycosylation, also raised WFS1 mRNA levels, suggesting that UPR increases WFS1 mRNA levels. However, the WFS1 protein level is not increased by tunicamycin. Subsequent analyses demonstrated protein stability to be reduced in the glycosylation-defective WFS1 protein. These results contribute to further understanding of the functions of this enigmatic protein.

Materials and methods

Reagents and antibodies. Tunicamycin, thapsigargin, DTT, and anti-actin antibody were purchased from Sigma–Aldrich Japan (Tokyo, Japan). Anti-HA and anti-CHOP antibodies were obtained from Santa Cruz Biotechnology (Santa Cruz, CA). Anti-WFS1 N-terminus antibody was described previously [11].

Pancreatic islet isolation and treatment with ER-stress inducers. Pancreatic islets were isolated from male C57BL/6 mice by retrograde injection of collagenase (Sigma–Aldrich Japan, Tokyo, Japan) into the pancreatic duct. Approximately 100 (for Western blot analyses) or 200 (for RNA extraction) islets were treated with 2 μg/ml thapsigargin, 5 mM DTT, or 5 μM tunicamycin for 36 h in RPMI1640 medium. Total RNA was extracted using Isogen reagent (NipponGene, Toyama, Japan). Quantitative real-time PCR analysis for WFS1 mRNA levels was performed using primers, 5′-CTGGAAACTCAACCCCAAGA-3′ and 5′-TTGGATTCACTGCTGACGAG-3′.

Plasmids. pHA-mWFS1 encodes a fusion protein consisting of an initiator methionine, the HA epitope tag (YPYDVPDYA), and amino acids 2–890 of mouse WFS1 protein. To generate this plasmid, a fragment encoding a *Sal*I restriction site and amino acids 2–484 was amplified by PCR. Using the PCR method, pmWFS1-HA encoding mouse WFS1 protein with an HA tag between residues 830 and 831 was also generated. pHA-mWFS1(N633D) and pHA-mWFS1 (N748D), which encode HA-tagged WFS1 protein with a mutation of asparagine 633 to aspartate and asparagine 748 to aspartate, respectively, were generated using PCR-based mutagenesis on pHA-mWFS1. pHA-mWFS1(N633D/N748D) encoding a mutant protein with mutation of both asparagine residues was generated using pHA-mWFS1(N633D).

Cell culture and transient transfection. MIN6 [12] and COS7 cells were grown in Dulbecco's modified Eagle's medium (DMEM) supplemented with 10% (v/v) fetal calf serum, 50 U/ml penicillin, and 50 μg/ml streptomycin sulfate. Transfection of plasmids was carried out using FuGENE6 (Roche, Indianapolis, IN) diluted in OPTI media (Invitrogen, Carlsbad, CA). Cells were harvested for Western blot or proceeded to immunostaining analysis 36 h after transfection. Immunostaining was performed using anti-HA antibody and FITC-conjugated anti-mouse IgG (Jackson ImmunoResearch, West Grove, PA).

Trypsin treatment. COS7 cells transfected with either pHA-mWFS1 or pmWFS1-HA were homogenized in a buffer containing 270 mM sucrose, 2 mM EDTA, and 50 mM Hepes (pH 7.5). Cellular membranes were recovered by centrifuging the homogenate at 17,400*g* for 15 min. Membranes (100 μg) were then incubated with trypsin at various concentrations at 4 °C. After a 30 min incubation, homogenates were boiled and subjected to SDS/PAGE and Western blot analysis.

Endoglycosydase cleavage. COS7 cells transfected with either wild-type WFS1 cDNA or mutant constructs were dissolved in denaturing buffer (0.5% SDS, 1% β-mercaptoethanol), boiled for 10 min at 100 °C, then incubated at 37 °C for 1 h with endoglycosidase H (500 U), and subjected to electrophoresis on NuPAGE 3–8% Tris–acetate gel (Invitrogen).

Metabolic labeling. MIN6 cells were labeled with [^{35}S]methionine and [^{35}S]cysteine (100 μCi/ml; EXPRE^{35}S^{35}S labeling mix, Perkin–Elmer-New England Nuclear, Boston, MA) in DMEM with either methionine or cysteine in the presence or absence of 5 μg/ml tunicamycin for 3 h. Cells were then chased for different periods in complete medium with or without tunicamycin. COS7 cells transfected with pHA-mWFS1 or pHA-mWFS1(N633D/N748D) were also labeled with [^{35}S]methionine and [^{35}S]cysteine for 3 h. Cells were then chased for different periods in complete medium. MIN6 and COS7 cells were lysed in a buffer containing 100 mM NaCl, 0.5 mM EDTA, 20 mM Tris (pH 7.5), and 0.5% NP-40. Lysates were incubated with 10 μl protein A/G–Sepharose (Amersham Biosciences, Piscataway, NJ) for 2 h and then briefly centrifuged. The resulting supernatant was incubated with anti-WFS1 N-terminus or anti-HA antibodies overnight and then incubated with protein A/G–Sepharose for 2 h. The beads were washed three times and bound WFS1 proteins were eluted in SDS-sample buffer and subjected to SDS/PAGE (10%).

Statistical analyses. Data are presented as means ± SE. Differences were assessed by Student's *t* test.

Results and discussion

Effect of ER-stress inducers on WFS1 expression in pancreatic islets

We recently reported that WFS1-deficient islets exhibited increased susceptibility to apoptosis due to impaired ER function [7]. Therefore, in this study, we first determined WFS1 expression in isolated mouse pancreatic islets treated with the ER-stress inducers, thapsigargin, DTT, and tunicamycin. Thapsigargin is an inhibitor of the sarco(endo)plasmic reticulum Ca^{2+} pump and

depletes ER Ca^{2+}, which affects the functions of Ca^{2+}-dependent ER chaperone proteins. DTT and tunicamycin affect protein folding by disrupting disulfide bonds and inhibiting N-glycosylation, respectively. These compounds therefore cause mis-folding of proteins (ER-stress) and induce UPR [13]. As shown in Fig. 1, WFS1 protein expression was increased in islets treated with 2 μM thapsigargin (Fig. 1A) or 5 mM DTT (Fig. 1B) for 36 h. Greater than threefold increases in WFS1 mRNA levels were also observed by quantitative RT-PCR analyses in islets treated with these agents (data not shown). Another ER-stress inducer, tunicamycin (5 μg/ml), did not raise WFS1 protein levels in isolated islets (Fig. 1C). However, quantitative RT-PCR analyses revealed WFS1 mRNA levels to be increased by 72% in islets treated with tunicamycin (Fig. 1D). These data suggest that WFS1 mRNA expression increases in response to the ER-stress.

WFS1 protein has been shown to be a glycoprotein [1] like the inositol trisphosphate receptor, another ER membrane resident protein essential for cellular calcium homeostasis and signaling [14]. The unaltered WFS1 protein levels despite increased mRNA levels in islets treated with tunicamycin raise the possibility that inhibition of N-glycosylation affects WFS1 protein stability. To address this possibility, pancreatic β-cell derived MIN6 cells were labeled for 3 h with [^{35}S]methionine/cysteine and chased with unlabeled methionine and cysteine for different intervals in the continuous absence or presence of tunicamycin. As shown in Fig. 1E, WFS1 protein in tunicamycin-treated cells was more rapidly degraded, suggesting that inhibition of N-glycosylation reduces WFS1 protein stability.

Membrane topology of WFS1 protein

To study the roles of N-glycosylation more specifically, we first sought to determine N-glycosylation site(s) of WFS1 protein/wolframin. Since N-glycosylation occurs in the ER, it was prerequisite to know the membrane topology of this protein. The initial hydropathy plot studies did not provide a definitive answer; WFS1 protein contains 9 or 10 transmembrane segments, with long hydrophilic stretches on both the N- and the C-termini [2,3].

To localize the N- and the C-termini of WFS1 protein with respect to the ER membrane, we transiently expressed, in COS7 cells, mouse WFS1 protein tagged with an HA-epitope in either the N- or the C-terminal stretch (designated HA-mWFS1 or mWFS1-HA, respectively,

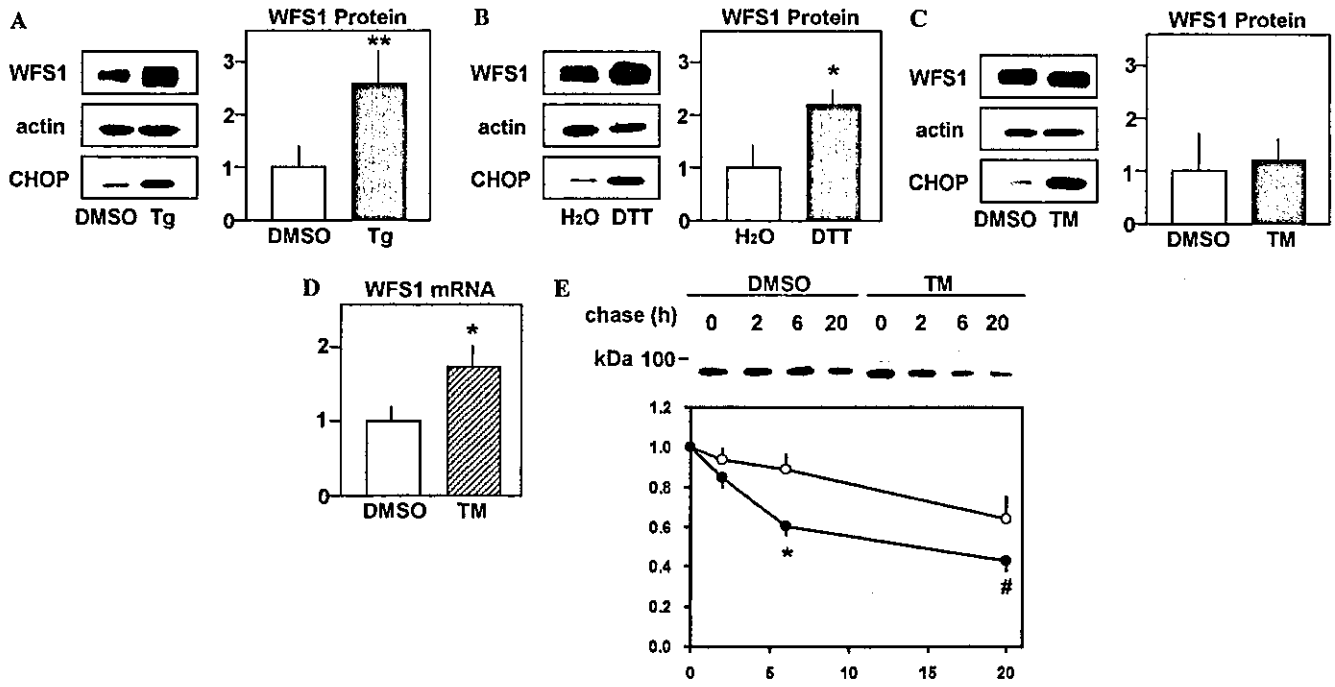

Fig. 1. WFS1 expression in mouse pancreatic islets in response to ER-stress inducers. (A–C) Isolated mouse islets were challenged with 2 μM thapsigargin (Tg) (A, $n = 4$), 5 mM DTT (B, $n = 3$) or 5 μg/ml tunicamycin (TM) (C, $n = 5$). After a 36-h incubation, the islets were subjected to SDS/PAGE and blotted using antibodies against the WFS1 N-terminus, actin, or CHOP. Representative blots are shown in the left panels. Increased CHOP expression indicated successful induction of ER-stress mediated apoptosis. WFS1 protein/actin levels are summarized in the right panels. Data are expressed as the expression relative to those of a control islet preparation. (D) Total RNA was extracted from isolated mouse islets treated with 5 μg/ml tunicamycin for 36 h. WFS1 and GAPDH mRNA levels were determined by quantitative real-time PCR. WFS1 mRNA levels were normalized to those of GAPDH. Data were obtained using three independent sets of islet preparations. (E) MIN6 cells were pulse-labeled for 3 h without or with 5 μg/ml tunicamycin and chased for up to 20 h in the continuous absence or presence of the drug. A representative result from three independent experiments is shown in the upper panel. Data from three experiments are summarized, after normalization to time zero of the chase in the lower panel. Open circles, DMSO-treated MIN6 cells. Closed circles, tunicamycin-treated cells. $^{\#}P = 0.0634$, $^{*}P < 0.05$, $^{**}P < 0.01$.